2018

Structural and Chemical Consequences of High Oxygen Coverages on Rh(111)

Rachael Gabrielle Farber
Loyola University Chicago

LOYOLA UNIVERSITY CHICAGO

STRUCTURAL AND CHEMICAL CONSEQUENCES OF HIGH OXYGEN COVERAGES ON RH(111)

A DISSERTATION SUBMITTED TO

THE FACULTY OF THE GRADUATE SCHOOL

IN CANDIDACY FOR THE DEGREE OF

DOCTOR OF PHILOSOPHY

PROGRAM IN CHEMISTRY

BY

RACHAEL G. FARBER

CHICAGO, IL

MAY 2018

ACKNOWLEDGMENTS

I would like to acknowledge the many individuals who have made the completion of this dissertation possible.

First, I must thank my advisor and committee chair, Dr. Dan Killelea. Dr. Killelea has been an invaluable support during my time at Loyola University Chicago. This work would not have been possible without his guidance, encouragement, and leadership. As well as being a magnificent mentor in lab, Dr. Killelea has continually pushed me to develop as a scientist, mentor, and individual. I am incredibly grateful for his support and friendship, and I would not have been able to achieve what I have without his influence. I would also like to thank the other members of my dissertation committee for their time and commitment to my professional development: Dr. Patrick Daubenmire, Dr. Jacob Ciszek, Dr. Daniel Graham, and Dr. Michael Trenary.

I would also like to thank the other members of Dr. Killelea's group. My predecessor, Dr. Jon Derouin, for his guidance and friendship during my first few years at Loyola, as well as current graduate student, Marie Turano, for her friendship and assistance on the projects discussed herein. The assistance of the undergraduates in the group, specifically Eleanor Oskorep and Noelle Wands, is also greatly appreciated. These women have not only assisted in the work presented, but have also become dear friends.

Additionally, I would like to thank the Loyola University Chicago Chemistry Department for their support during my graduate studies. Matt Sara has been very tolerant these past five

years with the numerous liquid nitrogen fill requests, without which the lab would be at a standstill. I would also like to thank Denise Hall, Carol Grimm, and Sandy Orozco for their help over the years. I would also like to thank the Arthur J. Schmidt Foundation for the fellowship that has allowed me to complete my research during my final term.

I have also been extremely fortunate in the connections I have made outside the Loyola Chemistry Department. Dr. Charlie Sykes has been a wonderful advocate and mentor, and I am very glad I have had him as a resource. Dr. Erin Iski, visiting professor and honorary group member, has helped hone my imaging abilities, is a wonderful mentor, and I am glad I have her as a friend. I would also like to thank Dr. Jason Weaver for the opportunity to visit and work with his group, as well as his guidance. The collaborations between the Killelea group and Dr. Ludo Juurlink's group has been fruitful in more ways than one. Dr. Juurlink insight into science has been eye opening, and his advice and support during my postdoc search was invaluable. I would also like to thank Dr. Juurlink for the opportunity to work with Dr. Manuel Kolb on my first project in Dr. Killelea's group, as well as the opportunity to work with Dr. Cansin Badan for a second collaboration. As a result of my contact with Dr. Juurlink's group, I have also had the opportunity to meet Sabine Auras and Richard van Lent. In addition to the project we are currently collaborating on, Sabine and Richard have become dear friends, and I am very lucky to have met them. I would also like to thank Dr. Alex Kandel for lending the Killelea lab a LEED; it has been a central part of several of my publications.

Finally, I must extend my sincerest thanks to my friends and family that have supported me throughout my graduate studies. My friends have dealt with cancelled plans and frantic texts and Snapchats for the entirety of my graduate studies, and I am so thankful for their support during everything. My parents, Doug and Rosetta Farber, and sister, Sara Farber-Smigel, have

always been my biggest cheerleaders, and their support over the years has been invaluable. Mark Schultz, my husband, has stood by me for every Progress Committee Meeting, paper draft reading, and practice talk, and his love and dedication has been a constant through everything. I would also like to thank Bob and Tina Schultz, as well as Emma Schultz, for their support during my program. The emotional support I have received from my loved ones during my graduate studies have made everything possible, and I would not be here without them. Last, but certainly not least, I must acknowledge my ever-present support animals, Appa the Wonder Corgi and Shadow the Mrowsiest Cat Ever.

TABLE OF CONTENTS

LIST OF FIGURES

LIST OF ABBREVIATIONS

AES	Auger electron spectroscopy
Ag	Silver
AO	Atomic oxygen
Ar	Argon
CO	Carbon monoxide
CO_2	Carbon dioxide
K	Kelvin
L	Langmuir
LEED	Low energy electron diffraction
ML	Monolayer
NO_2	Nitrogen dioxide
O_2	Molecular oxygen
$O_{2,chem}$	Chemisorbed molecular oxygen
O_{ad}	Adsorbed oxygen
O_{res}	Residual oxygen
O_{sub}	Subsurface oxygen
Pt	Platinum
Pd	Palladium
QMS	Quadrupole mass spectrometer

RGA	Residual gas analysis
Rh	Rhodium
RhO_2	Rhodium surface oxide
s	Second
S_0	Sticking probability
STM	Scanning tunneling microscopy
T_{dep}	Deposition temperature
T_s	Surface temperature
TPD	Temperature programmed desorption
$\theta_{O,ad}$	Surface oxygen coverage
$\theta_{O,surface}$	Surface oxygen coverage
$\theta_{O,total}$	Total oxygen coverage
θ_O	Total amount of oxygen
UHV	Ultra-high vacuum
UHV-STM	Ultra-high vacuum scanning tunneling microscopy

ABSTRACT

Partial oxidations of small molecules over metal surfaces are central to many heterogeneously catalyzed reactions. However, the identity of the actual surface species that promote or hinder these reactions has remained elusive for a variety of reasons. Recently, the understanding of the role of surface oxides in catalytic activity has changed. Instead of being thought of as poisons, they are now believed to be effective promoters of selective catalysis.

Rh(111) was chosen as a model system to study oxidation; Rh effectively promotes oxidation reactions and is a benchmark system for models of heterogeneously catalyzed chemistry. In this dissertation work, the uptake of oxygen on Rh(111) was fully characterized for coverages from 0.5 monolayers (ML) to over 8 ML. The surface oxygen coverage was determined with Auger electron spectroscopy (AES), total oxygen abundance with temperature programmed desorption (TPD), and the surface structures with low energy electron diffraction (LEED) and scanning tunneling microscopy (STM).

Careful control of the exposure parameters allowed for the selective growth of the RhO_2 surface oxide, surface adsorbed oxygen, and subsurface oxygen. Following surface oxide growth, the Rh crystal was exposed to carbon monoxide (CO) to study CO oxidation as a probe reaction. Carbon dioxide (CO_2) yield was measured using TPD and surface structure evolution was tracked using STM. This is the first study that shows atomically resolved structural information regarding CO oxidation on RhO_2, and reveals conclusive structural evidence of low temperature CO oxidation on RhO_2 under UHV conditions.

CHAPTER ONE

INTRODUCTION

Heterogeneously catalyzed chemical reactions are ubiquitous in nature; molecules in the interstellar medium are formed via surface-mediated processes, and icy surfaces process molecules in the terrestrial atmosphere. In heterogeneous catalysis, the catalyst and reactants are in different phases, and the catalyst is used to increase the rate of a chemical reaction by lowering the activation energy needed for the desired products to form. Heterogeneous catalysis has greatly impacted industrial synthetic applications; creating an energetically favored reaction pathway allows for the selective formation of desired products. Utilized in the formation of plastics, prescription medicines, and chemicals for further industrial and research use, heterogeneous catalysis is used in the formation of over 90% of manufactured products[2]. Besides their synthetic utility, heterogeneously catalyzed reactions may also have positive environmental and societal impacts in abating pollution; heterogeneously catalyzed reactions have been a major component in continued efforts to reduce the disastrous consequences of human induced climate events.

From the 1940s through the 1970s, Los Angeles had some of the most polluted air in the world. The level of smog, a combination of nitrogen oxides (NO_x) and hydrocarbons (HC), resulting from automobile exhaust made residents of the city unable to venture outside without experiencing headaches, shortness of breath, and other environmentally induced illness. Eugene Houdry, a French mechanical engineer who emigrated to the United States in 1930, saw the

effects of factory and automobile exhaust on the air quality in Los Angeles, and began developing catalytic converters at the Oxy-Catalyst Company in the 1950s to neutralize the toxicNO_x and HC emissions from automobile and factory exhaust fumes[3]. In the mid-1970s, when the EPA began enforcing more stringent emission regulations and requiring catalytic converters to be installed on all manufactured automobiles, the air quality of Los Angeles began to improve dramatically. Modern catalytic converters are made of a combination of platinum (Pt), palladium (Pd), and rhodium (Rh). This trio of metals is referred to as a three-way catalytic converter, and utilize each metal to effectively reduce or oxidize noxious exhaust into more benign emissions. In the case of the catalytic converter, heterogeneous catalysis serves to not only neutralize emissions from automobiles, but is the reason why air quality in Los Angeles, and many cities around the world, is now acceptable.

In heterogeneous catalysis, such as NO_x and HC oxidation/reduction via the three-way catalytic converter, the chemical species present on the catalyst surface, and resultant surface structure, are essential for product formation and reaction efficiency. For many heterogeneously catalyzed reactions, however, the active surface species are poorly defined. By understanding the active surface structure or species present during reaction conditions, optimal reaction parameters can be obtained to form the desired chemical product.

The oxygenaceous species on oxidized metal surface of a heterogeneous catalyst is of particular importance in determining catalytic function. Due to the varying attractive and repulsive interactions among adsorbed oxygen and the metal surface, a variety of oxygen species, and thus structures, may be present on the catalyst surface. These oxygen species may include adsorbed O_2, adlayers of adsorbed O atoms (O_{ad}), surface reconstructions, surface

oxides, and bulk oxides. Each of these oxygen phases results in a unique chemical state for the oxygen and metal, in turn indicating surface reactivity[4-5]. When the interaction between an O_2 molecule and the surface are relatively weak, the O_2 will adsorb intact, often at low temperatures. In these instances, the O_2 is weakly bound to the surface via physisorption[6]. For O_{ad}, the interaction between the O_2 molecules and surface are significantly stronger than for physisorbed O_2. This results in the O_2 bond breaking, forming dissociatively adsorbed O_{ad} which is chemisorbed to the surface[7]. The strength of interaction between the chemisorbed O_{ad} and the surface allows for O_{ad} to be present at much higher temperatures than physisorbed O_2. As interactions between the surface and adsorbate increase, the metal lattice restructures itself to accommodate the new O atoms. This is especially prevalent in Ag oxidation; a variety of coexisting surface reconstructions form due to the interaction between O_{ad} and surface Ag atoms[8-9]. As oxygen coverage increases on the metal surfaces, the metal shifts from metallic to oxide[10]. This shift in nature of the metal surface also alters the adsorbate surface interactions; the chemical nature of O_{ad} goes from ionic to covalent[11-12]. In this regime, structures such as surface oxides, thin films of oxide, and bulk oxides are able to form[13]. Rh surface oxide, RhO_2, has a trilayer O-Rh-O stacking structure. The chemical identity of the oxygen is unique to the surface oxide, and the upper and lower oxygen layers have unique chemical identities from one another[14]. The Rh in this trilayer is also distinctly different from bulk Rh; there is evidence of strongly oxygen coordinated Rh which is only found when the surface oxide is present coexisting with metallic Rh[1]. Bulk oxides are thicker oxide layers on the metal surface. When bulk oxides are present, there is no metallic identity remaining, only evidence of metal that is strongly coordinated to oxygen[15]. Because of the unique chemical identities of surface and bulk oxides

from one another, and the metallic surface, the chemical reactivity varies drastically for each surface species.

In addition to the various surface phases of oxygen on metals, oxygen dissolved into the top few layers of the metal crystal, or subsurface oxygen, has recently been suggested as an important oxygen phase for heterogeneously catalyzed reactions[16-17]. Less is known, however, about the chemical characteristics and structural effects of subsurface oxygen on surface structure and function than the aforementioned oxygen phases. Consequently, recent studies have begun to investigate the properties of dissolved oxygen in catalytic metal surfaces.[18]

This central relationship between structure and function has resulted in many fundamental surface science studies of catalytic transition metal single crystals under ultra-high vacuum (UHV) conditions. Working under pressures 12 to 13 orders of magnitude below atmospheric pressure, the interactions between specific adsorbed molecules and the native metal surface have been well defined for several benchmark systems[7, 19-20]. Actual heterogeneously catalyzed reactions, however, usually require elevated temperature and high-pressure conditions, resulting in high adsorbate coverages and complex surface interactions. The discrepancy between actual reaction conditions and UHV conditions is often referred to as the "pressure gap"[21]; this makes direct comparisons between the surfaces present in vacuum to those in actual catalysis challenging. The key is to find the essential aspects of the complex catalytic surfaces and reproduce them under UHV conditions for detailed study**.** The ability to discern the reactivity of catalytically relevant surface species or structures present during reaction conditions would be a significant advance in understanding the fundamental chemistry of metal surfaces in catalysis. Recent developments in surface science analysis techniques have allowed for the study of metal

surfaces under more realistic pressures[22-24]. High-pressure surface x-ray diffraction (SXRD)[25], ambient pressure x-ray photoelectron spectroscopy (AP-XPS)[26-28], scanning electron microscopy (SEM) and transmission electron microscopy (TEM) of nanoparticles[29], and high-pressure scanning tunneling microscopy (STM)[22, 24, 30] have revealed the dynamic properties of solid catalysts, but such preparation methods result in complex mix of surface phases[25, 31].

Although there was a time when oxide surfaces were though to be inert, our understanding of them has changed over the past decade or so. It is clear now that oxide surfaces may be highly active, but this reactivity may strongly depend on the exposed facet or interface with the metal. Despite the complexity of the resultant surfaces, researchers have determined that surface oxides are a crucial part of catalytic activity[1, 12, 17, 32-35]. While surface oxides have been identified as catalytically relevant, atomistic information is difficult to obtain from such high-pressure preparation methods due to the increased complexity of the system. Consequently, atomically resolved structural characterization is still needed for the prepared catalytically relevant surfaces. Such atomic characterization is, however, only possible under UHV conditions. As such, a method to prepare catalytically relevant surface species under UHV conditions is necessary to characterize the active surface phase.

This dissertation work has focused on revealing a straightforward, UHV based, approach to prepare the Rh(111) surface with high oxygen coverages akin to those present under reaction conditions. Using gas-phase atomic oxygen (AO), we have developed a preparation method that combines the relevant surface oxide with controlled reaction conditions found under UHV conditions. Using temperature programmed desorption (TPD), Auger electron spectroscopy (AES), and low energy electron diffraction (LEED), ensemble surface chemical and structural

information was obtained to characterize surface wide behavior. Low-temperature STM was used to provide structural information not available from high pressure or temperature studies of catalytic metal surfaces. By using this combination of UHV techniques, the chemical and structural identity of the Rh(111) surface following AO exposure and CO oxidation provides atomic-scale information of a catalytically relevant metal surface.

Rhodium

Rhodium is a powerful and selective catalyst for a variety of applications including the oxidation of small molecules and NO_x reduction[34, 36-38]. The chemical species and surface structures present on catalytic metal surfaces greatly influences the chemical efficacy of the

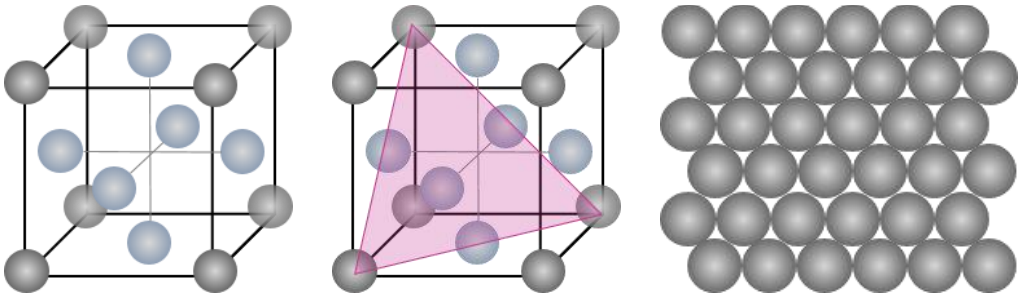

Figure 1. Left) The face centered cubic (fcc) unit cell structure; Center) The (111) plane of an fcc unit cell; Right) a representative, atomically flat fcc (111) surface.

catalyst as well as the resultant chemical product. Due to the many applications of Rh in heterogeneously catalyzed reactions, there have been many studies to discern fundamental adsorbate-surface interactions on Rh under UHV conditions[39-43]. Rh has a face centered cubic (fcc) crystal structure as shown in Figure 1. To simplify adsorbate-surface interactions, many studies have used the (111) face of the Rh crystal. This denotation, known as a Miller index, specifies the manner in which the bulk crystal is cleaved to generate a particular surface structure. In the instance of Rh(111), the three axis of the bulk crystal are intersected, resulting in

an atomically flat surface termination (Figure 1). Such a truncation limits the number of undercoordinated step edge atoms, controlling the interactions between adsorbates and surface defects.

Along with Miller indices, Wood's notation is a commonly used method of classifying overlayer structures on single crystal surfaces. The primitive unit cell of an fcc (111) surface, the smallest possible repeating unit of the surface, is defined by identifying the substrate vectors that, when repeated in an ordered array, generates the surface structure, as shown in the left image of

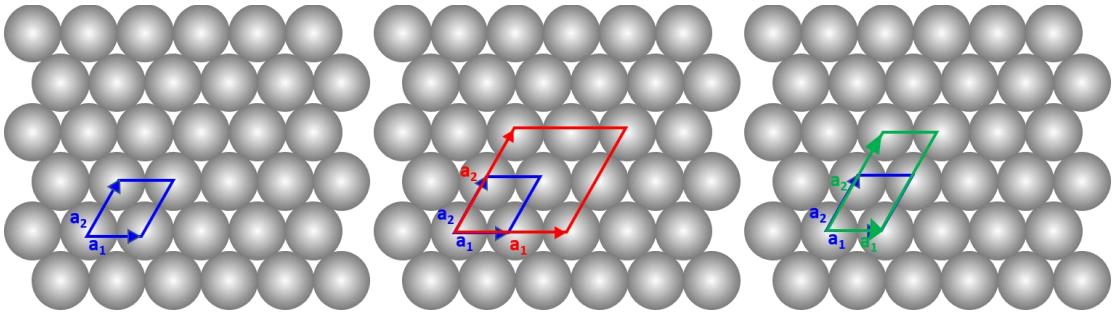

Figure 2. Left) The (1×1) unit cell on an fcc (111) surface; Center) The (2×2) unit cell in red; Right) The (2×1) unit cell in green.

Figure 2. For the fcc (111) surface, the unit cell is (1×1). Surface adlayers are identified relative to the native (1×1) surface cell. When the adlayer has a spacing that is twice the size of the unit cell in both directions, the adlayer unit cell is then referred to as (2×2), as shown in the center image of Figure 2. Similarly, a unit cell that is twice as long in one direction relative to the native unit cell, but the same size in the other direction, is defined as a (2×1) unit cell.

The use of Rh as a partial oxidation catalyst has resulted in many studies investigating the interaction of oxygen with Rh(111)[41, 43-44]. Despite the seeming simplicity of the O/Rh(111)

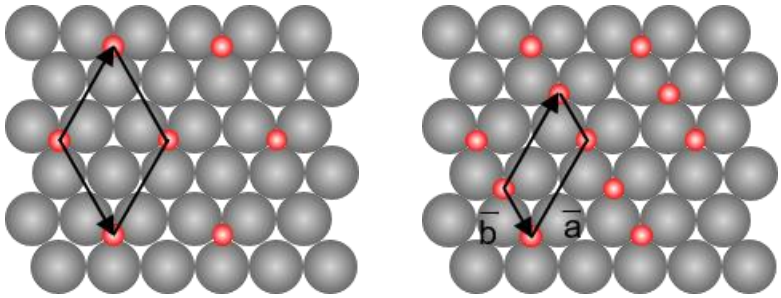

Figure 3. Left) The (2×2)-O adlayer on Rh(111); Right) The (2×1)-O adlayer on Rh(111)

system, much effort went into determining the structure of adsorbed oxygen (O_{ad}) on Rh(111). Early work using LEED showed that the Rh(111) surface saturates upon the formation of a (2×2)-O overlayer[45-46], depicted in the left image of Figure 3. Subsequent work showed that it would be impossible to distinguish the (2×2)-O surface structure from three domains of (2×1)-O rotated by 60˚, depicted in the right image of Figure 3[47]. Once STM was used to investigate the O/Rh(111) surface, it was determined that the predominant surface structure upon saturation with O_{ad} was the (2×1)-O adlayer[40, 43]. The model for O_{ad} on Rh(111) under UHV conditions now shows that the surface is covered in the (2×2)-O adlayer that has a coverage (θ_O) of 0.25 monolayers (ML) at low coverages. As coverage is increased, the surface saturates at 0.5 ML, which corresponds to the (2×1)-O adlayer. The 0.5 ML is kinetically limited due to O_2 needing two adjacent vacant sites on the Rh surface to dissociate under UHV conditions.

When Rh(111) is exposed to high O_2 pressures[1] or gas phase AO[48] at elevated temperatures, the surface oxide forms along step edges and defect sites. The surface oxide

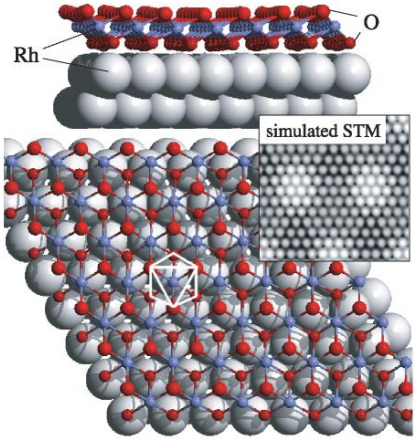

Figure 4. Side and top views of the Rh surface oxide, RhO_2[1].

displays in STM images as a moiré pattern; this is a result of the misfit between the 3.02 Å oxide lattice and 2.69 Å native Rh lattice[1]. A moiré pattern results from the constructive interference of two similar lattices overlaid with one another. The constructive wave interference from the two structures results in the formation of a larger projection of the combined structures. The Rh surface oxide, RhO_2, is a trilayer reconstruction of the Rh(111) surface. As show in Figure 4[1], a (7×7) O-Rh-O unit cell lies atop the native (8×8) Rh(111) surface supercell. The trilayer reconstruction is defined as such due to the sandwiching of Rh atoms between two layers of O atoms; due to the intermolecular interactions between the O and Rh atoms, the Rh(111) surface reconstructs to allow for the top layer of Rh atoms to integrate into the oxide structure. Whereas the surface oxide causes a reconstruction of the Rh(111) surface, the (2×2)-O and (2×1)-O adlayers are formed by O_2 dissociatively adsorbing onto Rh(111). As such, there is no reconstruction of the Rh(111) surface, and the O_{ad} is chemisorbed to the surface. While once

believed to be a catalyst poison or inactive spectator, the oxide surface is now believed to be catalytically active and crucial to catalyst function[4-5, 33, 49].

While fundamental interactions of small molecules, such as O_2 and CO, on metal single crystals have been thoroughly studied under UHV conditions, only recently have advances been made regarding surface structures present under actual high pressure and temperature conditions commonly found in actual heterogeneously catalyzed reactions[15, 50-51]. Utilizing high pressure O_2 exposures[1], AO plasma sources[52], and gas phase AO[48, 53] has allowed for the formation of surface structures that are not stable under UHV conditions. In CO oxidation studies in which the surface oxide is present on Rh nanoparticles and single crystal surfaces, CO_2 yield is significantly higher compared to the Rh surface that is solely covered in O_{ad}[10, 34, 49]. Recent work has also demonstrated the unique character of bulk oxides. Low-temperature activation of methane has been observed on bulk iridium oxide, $IrO_2(110)$[54], further supporting the enhanced catalytic activity of particular oxide species on metal catalysts. In doing so, it has been determined that catalytic activity cannot be attributed solely to the metallic phase.

In an effort to study the catalytically relevant surfaces using traditional UHV surface science techniques, this dissertation work focuses on forming high coverage oxygen adlayers and surface oxides on catalytically relevant transition metal surfaces. First, the effect of the metal surface on subsurface oxygen (O_{sub}) stability was probed by comparing Rh(111) to Pt(553), a highly stepped metal surface[55]. With the confirmation that the metal affinity for O_{sub} greatly contributes to O_{sub} formation, a reproducible method for forming various catalytically relevant oxygen phases on Rh(111) was determined[48]. While recent studies have shown catalytically relevant surface phases, the methods employed have made determining the exact site of

reactivity difficult to obtain. The last portion of this dissertation work has focused on determining the active site for CO oxidation on Rh(111) using TPD and STM to provide atomically resolved structural information. This crucial information will greatly improve our understanding of the surface reaction mechanism for CO oxidation on Rh catalysts.

CHAPTER TWO

EXPOSURE OF PT(553) AND RH(111) TO ATOMIC AND MOLECULAR OXYGEN: DO DEFECTS ENHANCE SUBSURFACE OXYGEN FORMATION?

Reprinted with permission from **Exposure of Pt(553) and Rh(111) to Atomic And Molecular Oxygen: Do Defects Enhance Subsurface Oxygen Formation?**, Rachael G. Farber, Marie E. Turano, Eleanor C. N. Oskorep, Noelle T. Wands, Ludo B. Juurlink, and Daniel R. Killelea, *Journal of Physics: Condensed Matter* **2017** *29* (16), 164002.

The adsorption of oxygen onto metal surfaces is central to many heterogeneously catalyzed reactions, and is a benchmark system for refinement of theoretical models of surface structure and chemistry [56-58]. On many transition metal surfaces, O_2 readily dissociates into adsorbed oxygen atoms (O_{ad}) that are incorporated into stable adsorbate structures or surface reconstructions. On both Rh and Pt surfaces, O_2 may chemisorb at low surface temperatures (T_s), but above 200 K O_2 dissociatively chemisorbs to the metal and only O_{ad} is observed[59-61]. However, when the metal surfaces are exposed to more potent oxidants, such as NO_2 or gas-phase atomic oxygen (AO), higher oxygen coverages are possible, and the total amount of oxygen exceeds what is present on the surface. Besides the formation of three-dimensional oxides, O can become dissolved into the near surface, or selvedge, of the metal and form subsurface oxygen (O_{sub}). When O_{sub} is plentiful, total oxygen abundances in excess of 1 monolayer (ML, defined as one adsorbate per surface metal atom, $\approx 1\times10^{15}$ O cm^{-2})[62] are

possible. Typically, there will be an oxidized surface layer and the remaining oxygen is O_{sub}. O_{sub} are thought to be an important factor in heterogeneously catalyzed reactions because its presence alters the geometric and electronic structure of the metal surface, in turn influencing the reactivity of the metal surface[16, 63-65]. Additionally, O_{sub} acts as a reservoir of O atoms that can participate in the reaction; this effectively generates a higher surface concentration of O and prolongs the catalytic activity of metal surfaces [18, 66].

The stability of O_{sub} and the response of the surface to its presence vary for many metal surfaces. On Pd surfaces, small concentrations of O_{sub} form Pd oxides, and multilayer Pd oxides are readily formed from gas-phase AO [52, 67]. In Ag(111) surfaces, O_{sub} is destabilized above 500 K, and small abundances (≈0.1 ML O_{sub}) cause extensive surface reconstruction[68]. Alternatively, Rh surfaces are far less sensitive to O_{sub}. On Rh(111), total coverages in excess of 2 ML O have been prepared using AO with the persistence of the θ_O = 0.5 ML (2×1)-O adlayer. Furthermore, despite the high abundance of oxygen absorbed into the selvedge of the metal, there is no evidence of bulk or surface oxide formation [60]. Finally, Pt surfaces appear to resist the formation of O_{sub}. Exposure of Pt surfaces to AO results in the formation of three-dimensional oxides that disorder the surface once θ_O > 0.5 ML; no appreciable amount of O_{sub} was observed to form [69].

It is also worth noting that on each metal their activity towards O_2 varies as well. Ag(111) is effectively inert to O_2, but Pt and Rh surfaces are far more reactive [6]. Pt surfaces with (111) geometry typically exhibit an initial sticking probability (S_0) around 0.4, which decreases with increasing θ_O, until the terminal coverage of θ_O = 0.25 ML is reached[62]; exposure to NO_2 can achieve $\theta_O \approx 0.75$, but the surface was disordered[61]. Rhodium surfaces are even more reactive

towards O_2, S_0 is near unity, the surface becomes saturated at θ_O = 0.5 ML [60, 70] and no further oxygen accumulation is observed unless high pressures of O_2 are employed[33, 71].

In all of the above cases, planar surfaces with low defect densities were used. Due to the increased reactivity and lattice perturbation at defect sites, it is reasonable to think that O_{sub} formation may be enhanced on a surface with a greater number of defects. On Pd(100), for example, defects were observed to facilitate the formation of O_{sub} from surface-bound oxygen atoms [72]. Pt, however, has proven to be resistant to O_{sub} formation, with small amounts of O_{sub} formed near step edges after repeated high temperature exposures to O_2 [62]. In order to determine the effect defects have on O_{sub} formation, a Pt(553) crystal, a stepped Pt surface with 4-atom wide (111) terraces and (110) step geometry, was used. By exposing the Pt(553) surface to gas-phase AO, the O_{sub} formation can be tracked to determine how defect sites enhance O_{sub} formation and stability. The comparison of Pt(553) to Pt(111) elucidates how step edges and defect density can facilitate the formation of O_{sub} on a metal where O_{sub} is otherwise not stable. In addition to comparing the Pt(553) oxygen uptake with Pt(111), we compare the metal to planar Rh(111) exposed to similar amounts of AO to determine how metal identity, despite a high defect density, affects the formation and stability of O_{sub}.

The experiments were performed using an ultra-high vacuum (UHV) apparatus that has been described in detail previously [60]. The apparatus is equipped with Auger electron spectroscopy (AES) for surface analysis, low-energy electron diffractometer (LEED) for structural characterization, and two quadrupole mass spectrometers (QMS) for temperature programmed desorption (TPD) experiments and residual gas analysis (RGA). The Rh(111) and Pt(553) samples were supplied by Surface Preparation Laboratories (SPL, Zaandam, NL) and

were cleaned by repeated cycles of Ar^+ sputter and annealing in UHV [73]. Surface cleanliness was verified with AES and LEED.

The Rh(111) or Pt(553) crystals were exposed to a mixture of gas-phase atomic oxygen (AO) and O_2 in the UHV preparation chamber at the prescribed exposure temperatures. AO was generated by dissociation of O_2 over a hot 0.25 mm diameter Ir filament [74-75]. The chamber was backfilled to 5×10^{-7} Torr O_2 and the filament brought to around 1 cm from the front face of the crystal. AES analysis of the surface after AO exposure show only the accumulation of O on the surfaces, as previously reported for Ag(111) [35]. The total amount of oxygen (θ_O) was determined by integration of the O_2 recombinative desorption peak in a TPD experiment. For all TPD data, the ramp rate was 3.0 K s^{-1}. The peak area of the self-limiting 0.5 ML O coverage on Rh(111) from O_2 exposure was used to calibrate the TPD peak areas. AES was used to quantify the oxygen surface coverage ($\theta_{O,ad}$) on Rh(111), but this was not possible on Pt(553) because of difficulty in systematically quantifying the intensity of the Pt Auger peaks.

In order to determine how Pt(553) will be affected by high oxygen coverages from exposure to AO, we first explored the uptake of oxygen from O_2 exposures. As shown in Figure 5A, O_2 readily adsorbed to Pt(553) at T_s = 300 K. For modest oxygen coverages (θ_O < 0.2 ML) , O desorbed in a broad feature around 800 K in the TPD experiment. As θ_O, was increased, the desorption feature at 800 K shifted towards a lower temperature, ~ 750 K, and saturated at ~ 180 L; this higher temperature desorption feature is attributed to O desorbing from (110) step edges [76]. After 180 L O_2 exposures, a lower temperature shoulder began to develop at roughly 650 K.

With a 600 L exposure, the 650 K peak, assigned to O desorption from (111) terraces [76], saturated and further O_2 exposures had no effect on desorption behavior. The TPD spectrum is nearly identical to a 0.25 ML O_{ads} spectrum reported previously with a TPD ramp a 1 K s^{-1} [59], and is in agreement with Parker, *et al.*[61]. The total oxygen coverage (θ_O) as a function of O_2 exposure is shown in Figure 6A. The surface saturated at θ_O = 0.25 ML, similar to previous reports of O_2 dissociation on Pt(553) [59]. These data show that, at T_s = 300 K, O_2 exposures only formed surface bound oxygen that saturated at θ_O = 0.25 ML, characteristic of the *p*(2×2)-O

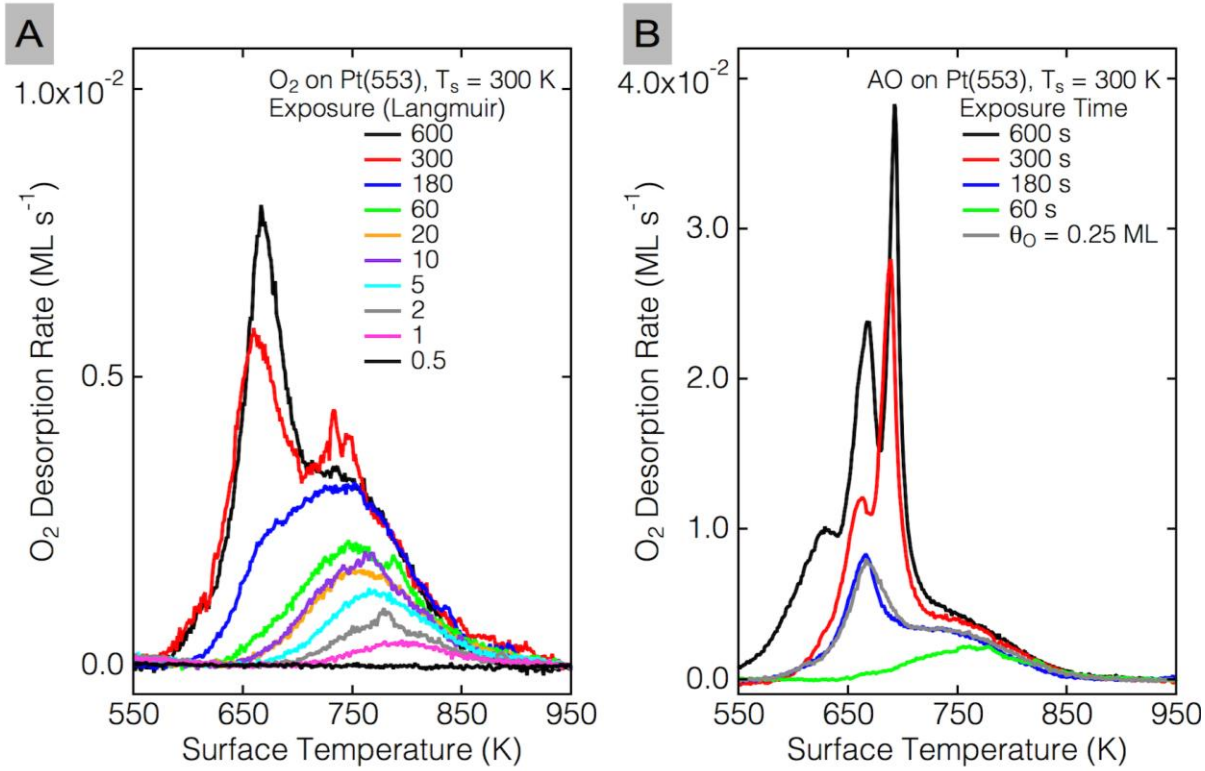

Figure 5. TPD spectra after oxygen desorption on Pt(553) at T_s = 300 K. Each spectrum was taken with a ramp rate of 3 K s^{-1}. A) desorption after various O_2 exposures. Terminal coverage was θ_O = 0.25 ML after 300 L dose. B) desorption after various AO exposures. In panel B, the two new peaks appear at ≈700 K and ≈625 K. The 700 K peak rapidly saturates indicating it is from a surface bound species while the 625 K peak is decomposition of the oxide.

adlayer. When comparing θ_O of Pt(111) and Pt(553), there is little difference between oxygen adsorption on the two surfaces [61, 77]. Although O_2 dosing at T_s = 300 K resulted in 0.25 ML saturation, it is important to note the effect T_s has on O uptake and desorption behavior. In a previous study we showed that significantly larger θ_O can be reached after extensive O_2 exposures at T_s = 100 K on Pt(553). The (110) step edge allows for the autocatalytic dissociation of O_2 into O_{ad} upon adsorption at 100 K resulting in a high location concentration of metastable chemisorbed molecular oxygen, $O_{2,chem}$, coexisting with O_{ad} at T_s = 100 K[59].

After characterizing O_2 uptake on Pt(553), we then studied the O uptake on Pt(553) after AO exposure. As shown in Figure 5B, the O_2 TPD peaks are still present, but after AO exposure two new desorption peaks were observed to form, one near 700 K and a second around 625 K. It is interesting to note that the smallest AO exposure (60s) roughly corresponds to a 60 L O_2 exposure, and integration of this peak yields a coverage of $\theta_O \approx 0.07$ ML. We used this to estimate the incident flux of AO impinging on the surface. Assuming the 1 cm diameter surface (A = 0.79 cm^2) was uniformly exposed to AO from the Ir filament, and the sticking probability of AO for $\theta_O < 0.1$ ML was unity, this yields a flux ($\Phi = \theta_O / A \bullet S_0 \bullet t$) on the Pt(553) crystal of Φ = 0.0015 ML cm^{-2} s^{-1} from the filament. This is in line with previous reports of AO generation from Ir filaments [74-75] and is less than 1% of the flux from the atomic beam source used by the Weaver group[69, 78].

As shown in Figure 6A, when AO exposure was increased, the TPD desorption features were initially similar to those seen for O_2 exposures. Like for O_2, the lower 650 K desorption peak grew in and appeared to saturate by a 180 s exposure, but thereafter θ_O surpassed the 0.25

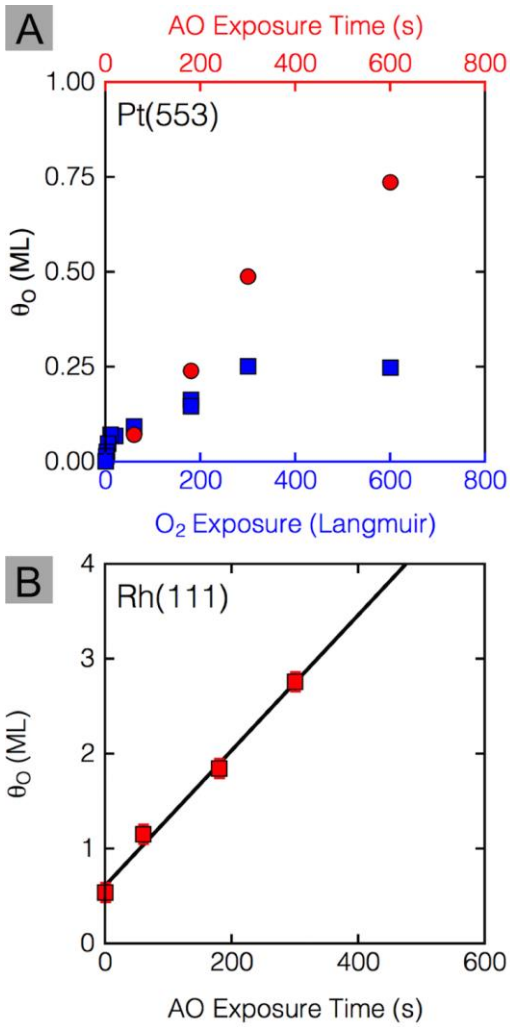

Figure 6. Integrated TPD area highlighting oxygen uptake as a function of exposure length. A) Direct comparison between oxygen coverage as a result of AO and O_2 exposure on Pt(553) B) Oxygen uptake after AO exposure on Rh(111).

ML and continued to grow, as evidence by the appearance of the two new desorption peaks. The new desorption peaks correspond to surface coverages in excess of 0.25 ML, as reported previously[61, 69]. The peak near 700 K is desorption from a (2×2)-O adlayer on the (111) terraces

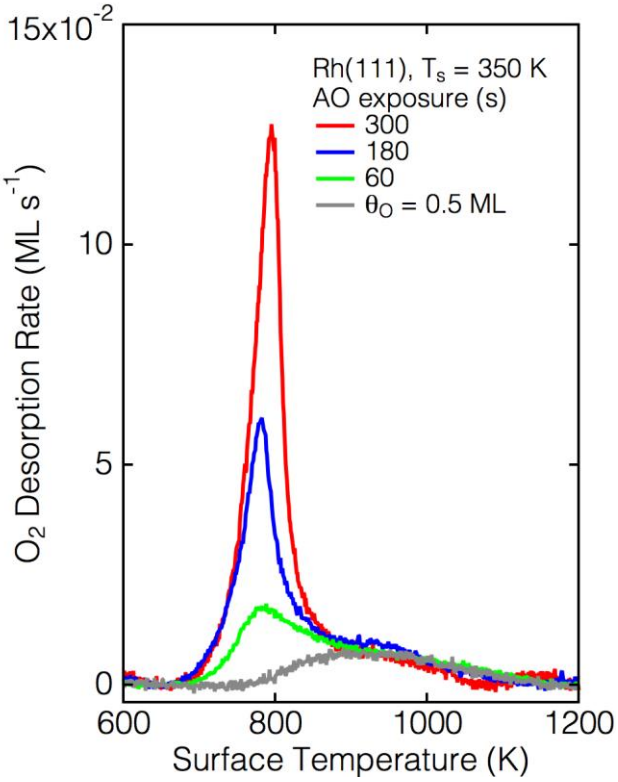

Figure 7. TPD spectra after exposure of Rh(111) to O_2 (θ_O = 0.5 ML) and AO with T_s = 350 K. All TPD data was collected with a ramp rate of 3 K s^{-1}.

and saturates at 0.25 ML[79]. At 600 s, a new peak develops around 625 K; the 625 K peak assigned to decomposition of platinum oxide, as previously reported by Weaver *et al.*[69, 78]. The evolution of the TPD desorption behavior corresponds well with surface evolution to allow for O uptake greater that 0.25 ML. Sharp desorption peaks at the same temperatures were also reported for high θ_O coverages of the very similar Pt(221) surface due to the autocatalytic dissociation of O_2 into O_{ad} at T_s = 100 K[59]. There was also a continuation in the O uptake, roughly 0.75 ML now

exist on the Pt(553) surface. While AO generated O uptake beyond 0.25 ML, there was still significantly less than 1.0 ML O on the surface. Previous work looking at Pt(111) after exposure to AO showed very similar results to those seen on Pt(553)[69]. From the TPD data alone, it appears as though the introduction of step edges did little to increase the stability and formation of O_{sub} on Pt, despite the rather high θ_O and presence of terrace step edges.

To see how Pt(553) O uptake after AO exposure compares to a different transition metal, we studied AO uptake on Rh(111). It is well known that on Rh(111), O_2 dissociates into O_{ad} and saturates at 0.5 ML forming a (2×1)-O adlayer. This 0.5 ML coverage, shown in Figure 7 as the gray TPD trace, has a characteristic broad desorption feature beginning at 800 K and continuing to 1200 K[70]. After exposure to AO, a sharp desorption feature at ~750 K grew in (Figure 7). As the length of exposure was increased, the ~750 K feature continued to grow, with no saturation point observed. The integrated TPD area also suggests O uptake would continue with further AO exposure. As shown in Figure 6B, the total θ_O on Rh(111) linearly increased, for example a 300 s AO exposure resulted in nearly 3 ML O uptake. The significant amount of O uptake, coupled with previous work identifying the sharp desorption feature after AO exposure as O_{sub} emergence[80], demonstrates that Rh(111) has a much higher affinity for O_{sub} formation, and subsequent, stability than Pt(553).

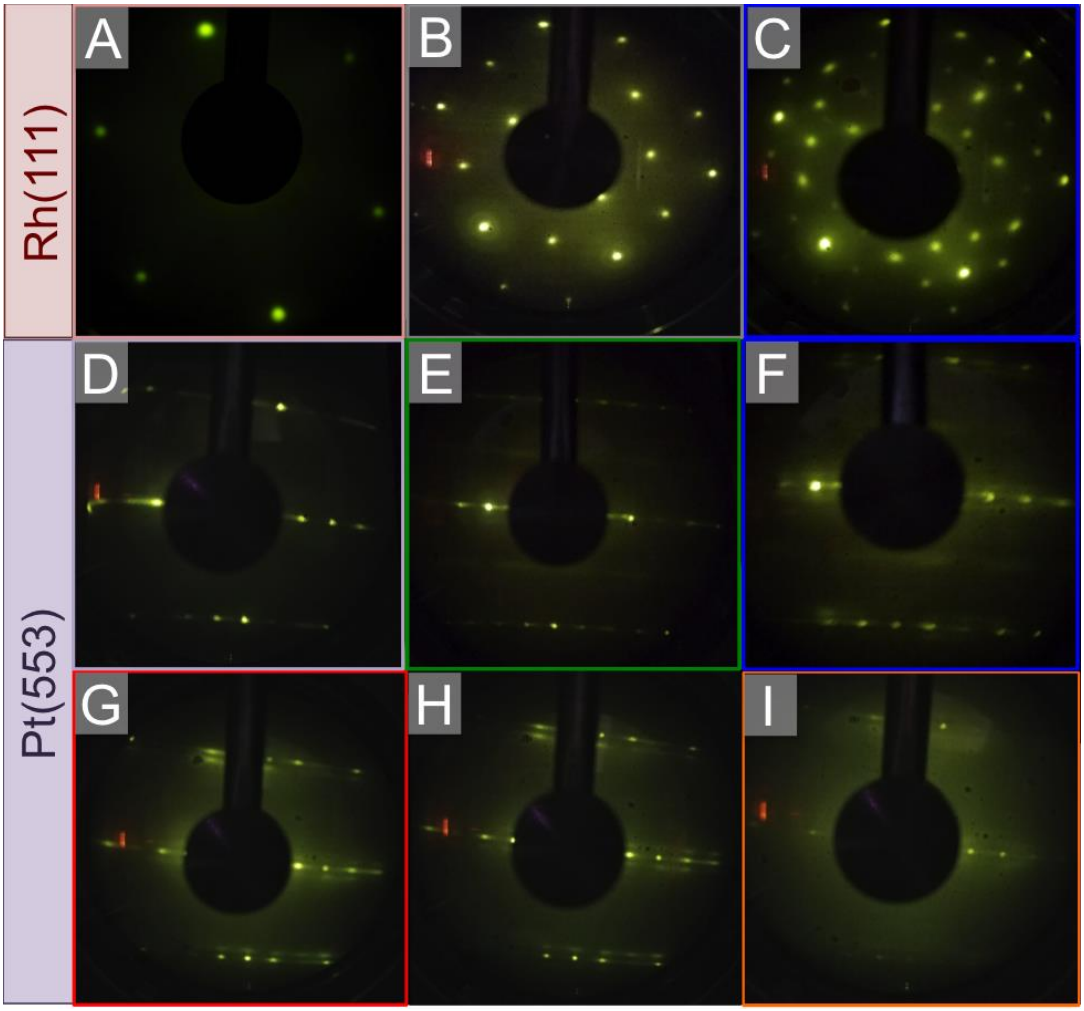

Figure 8. Images of LEED patterns on Rh(111) and Pt(553). Each pattern was obtained using 62 eV electron energy. A through C are LEED patterns of Rh(111) surface. D through I are LEED patterns of Pt(553) surface. The images from Rh(111) are: A) Clean Rh(111) showing (1×1) pattern; B) after 60 L O_2 exposure showing (2×1) pattern at θ_O = 0.5 ML O; and C) 180 s AO exhibiting (2√3 × 2√3) pattern. The lower six images are from Pt(553) and were taken after the following AO exposures: D) 0 s; E) 60 s; F) 180 s; G) 300 s; H) 600 s; and I) 1200 s. The degeneration of the pattern to a diffuse background is evident in panel I.

Using LEED, we were able to observe how the surface structure changed as more O was introduced into the system. Figure 8A shows a representative LEED pattern for a Rh(111) crystal. After a 60 L O_2 exposure (Figure 8B), a (2×1) pattern was present, indicating the formation of the (2×1)-O adlayer corresponding to 0.5 ML O_{ad}. After 180 s exposure to AO,

when the sharp desorption feature (Figure 7) is seen at 750 K on Rh(111), a ($2\sqrt{3}\times2\sqrt{3}$) pattern developed. This suggests that, after sufficient AO exposure and O_{sub} formation, the surface structure of the Rh(111) crystal changes in response to the presence of O_{sub}. On Pt(553), however, there was very little change in the surface structures detected after AO exposure. Figure 8D is a representative LEED pattern for a clean Pt(553) surface. Figure 8E-H shows the Pt(553) surface after 60, 180, 300, and 600 s AO exposures. The pattern shows very little change across the various exposures; the (2×2)-O adlayer shows as slight splitting of the native (553) surface, but otherwise there is no major surface structure change or reconstruction. After a 1200 s AO exposure (Figure 8I), however, the (553) structure is nearly obscured by a hazy background. This corresponds very well to work done by Weaver showing the degeneration of sharp LEED patterns as the surface became covered in three-dimensional patches of the bulk oxide, whose orientations develop stochastically and are incommensurate with the underlying Pt(111) surface[69, 78]. The progression of LEED patterns suggests that, while Rh(111) readily forms O_{sub} and has surface structure formations that represent that presence of O_{sub}, Pt(553) does not readily form O_{sub}. Instead, the Pt(553) surface forms a bulk Pt oxide after extensive AO exposure at room temperature, highlighting how the intrinsic stability of O_{sub} on a particular metal is more important than the defects that could facilitate the incorporation of oxygen into the selvedge.

While high θ_O coverages for Pt(553) may be obtained either through T_s = 100 K O_2 exposures or AO exposures at T_s = 300 K, neither oxidation process stabilizes the formation of O_{sub}. At low temperature O_2 exposures, a kinetic barrier allows for a supersaturation of $O_{2,chem}$ and O_{ad}, which forms due to step geometry effects[59]. While oxidation with AO at T_s = 300 K

does not experience such kinetic barriers for increased θ_O coverage, extensive AO exposure at 300 K results in bulk oxide growth rather than oxygen absorption into the selvedge. Rh(111), on the other hand, readily forms O_{sub} and the surface structures present evolve drastically in the present of absorbed O. These results suggest that, for Pt samples, defect sites alone are not enough to promote the formation of, and stability, of O_{sub}.

CHAPTER THREE

THE QUEST FOR STABILITY: STRUCTURAL DEPENDENCE OF RH(111) ON OXYGEN COVERAGE AT ELEVATED TEMPERATURE

The arrangements of atoms on oxidized metal surfaces arise from the interplay between attractive and repulsive interactions among the adsorbed oxygen atoms and the metal, resulting in a variety of surface structures. The surface structure of oxidized metals include adlayers, surface reconstructions, and surface oxides; these reveal the chemical state of both the adsorbed oxygen and the metal, and therefore are indicators of surface reactivity [4-5]. With increasing oxygen coverage (O atoms per surface metal atom), the oxidation state of the metal surface goes from metallic to oxide [10]. Concomitantly, the chemical state of the adsorbed oxygen shifts from ionic to covalent [11-12]. The surface structure also evolves with oxygen coverage; the structure is indicative of the chemical state of the oxidized surface, and thus, differs for various chemical states. When the chemical potentials of different oxidic phases are nearly isoenergetic, different surface oxygen phases co-exist on the surface [15, 81-82]. Proper identification of surface phases and their relative coverages provide insight into the fundamental chemistry of oxidized metal

surfaces. Understanding how metal surfaces respond to high coverages of oxygen is of particular importance for determination of the atomic-level nature of oxidation reactions over metal surfaces under the high-pressure conditions of industrial heterogeneous catalysis.[83]

Over the past decade or so, our understanding of the nature of the active surfaces in heterogeneous catalysis has significantly changed [10, 15, 84]. The paradigm of catalytic activity being solely due to the metal is incomplete; the oxide must also be considered. While once thought of as passive, or even a poison, it is now believed that the oxide surface is the catalytically important phase under reaction conditions for several major reactions [4-5, 33, 49]. Recently, atomic oxygen (AO) has been used to control the growth of high-quality oxide surfaces on Pt and Pd, allowing for thorough investigation of the physical and chemical properties of the oxidized surfaces [52-53, 85]. On Ag, the flux of AO was shown to be a key parameter in the growth of the oxide phase [35]. Similarly, exposing Rh(111) to high pressure O_2 yielded patches of a high-density oxygen reconstruction phase along with the surface oxide RhO_2 [1]. Although these studies clearly demonstrate the ability to form surfaces with coexisting oxide phases under strongly oxidizing conditions, the conditions for the growth of specific phases and their relative stability were not determined. In the present study, we show that exposing Rh(111) to gas-phase AO yields the same surface phases as high-pressure O_2 exposures, and that proper selection of deposition temperature (T_{dep}) and AO exposure yield particular surface structures. Despite total oxygen coverages ($\theta_{O,total}$) in excess of 5 monolayers of oxygen (ML, 1 ML = 1.6×10^{15} O atoms cm^{-2} [18]), the surface exhibited the (2×1)-O adlayer structure corresponding to an oxygen surface coverage ($\theta_{O,surface}$) of 0.5 ML. However, areas of the surface oxide (RhO_2) were

observed in the presence of defects and ample oxygen dissolved in the subsurface (or selvedge) of the metal.

The persistence of the (2×1) adlayer and the limited growth of the RhO_2 surface oxide are important for understanding the reactivity of Rh surfaces in catalysis. Ultra-thin RhO_2 oxide films on Rh metal surfaces have recently been cited as the chemically important surface in actual heterogeneous catalysis reactions [4, 49, 82]. The oxide surface structure is insensitive to the structure of the bulk metal, so the oxide observed on Rh(111) is relevant to the surface of oxidized nanoparticles [82]. Oxide formation on Rh nanoparticles increases the rate of CO oxidation and such catalytic activity is directly tied to the amount of oxide formed on the nanoparticle surface [34]. Despite the critical role surface oxide films play in catalysis, the energetic reasons behind the formation of certain surface oxide films are unclear, as are the factors that favor or disfavor their formation.

Herein, we characterize oxidized surfaces using ultra-high vacuum scanning tunneling microscopy (UHV-STM), temperature programmed desorption (TPD), Auger electron spectroscopy (AES), and low-energy electron diffraction (LEED). Furthermore, this approach allows for quantitative analysis of O uptake and directly connects oxygen exposure, uptake, surface coverage, and structure. These results show that the RhO_2 surface oxide and (2×1)-O adlayer are both thermodynamically stable. Finally, the surface oxide is not observed to form at lower deposition temperatures or on terraces, suggesting defects facilitate oxide formation at elevated temperatures.

Experiments were performed in an ultrahigh-vacuum scanning tunneling microscope (UHV-STM, RHK Technology, Troy, MI) apparatus described previously [60]. The STM has a

Pan-style scanner and is suspended from the bottom of a vibration-isolated closed-cycle He cryostat, which has a base temperature around 12 K. The Rh(111) crystal (Surface Preparation Laboratory, Zaandam, NL) was mounted on a Ta sample holder (McAllister Technical Services, Coeur d'Alene, ID) with a type-K thermocouple. Repeated cycles of Ar^+ sputtering and annealing at 1300 K prepared a clean Rh(111) surface; cleanliness was verified by Auger Electron Spectroscopy, a sharp (1×1) LEED pattern, and STM. Atomic oxygen (AO) was generated using a hot Ir filament as described by Umemoto, *et al* [74, 86]. The UHV chamber was backfilled with O_2 (g) to 5×10^{-7} Torr, and the hot Ir filament was positioned within ≈ 0.5 cm of the front face of the Rh(111) crystal. AES measurements showed no new peaks besides O, as previously reported [35]. LEED patterns were obtained with the Rh(111) crystal at 300 K. All TPD measurements used a ramp rate of 3 K s^{-1}, and the spectra were recorded with a UTI 100c quadrupole mass spectrometer controlled by a homebuilt labVIEW program. Prolonged O_2 exposure at 350 K yields 0.5 ML O_{ad}; the integral of the O_2 TPD peak from this surface was used to calibrate the total amount of O for other TPD experiments.[60] All STM images were taken at 30 K. Post-imaging TPD data showed neither accumulation of background gases [87] nor degradation of the oxidized surface. Likewise, LEED patterns taken before imaging were indistinguishable from the post-imaging patterns. LEED analysis did not alter the oxidized surface; both TPD spectra and STM images showed no discernable difference whether or not a LEED was obtained.

O atoms on the Rh(111) surface recombinatively desorb as O_2 in a TPD measurement, and integration of the desorption peak yields $\theta_{O,total}$. Figure 5 shows TPD spectra for O_2 desorption from Rh(111) after various exposures to gas-phase AO with the surface at either

T_{dep} = 700 K (Figure 9A) or T_{dep} = 350 K (Figure 9B). The O_2 desorption temperatures and peak shapes were nearly the same, suggesting that the O atoms were likely in similar adsorption and/or absorption sites after exposure at either temperature. Arrhenius analysis of the leading edges of the apparently zeroth-order desorption features [61] found the activation energies (E_a) for desorption to be 220 ± 6 kJ mol^{-1} for T_{dep} = 700 K and 201 ± 6 kJ mol^{-1} for T_{dep} = 350 K. This difference in E_a suggests the oxygen from higher T_{dep} was more stable, but the difference was modest. However, as shown in Figure 9C, T_{dep} had a pronounced effect on $\theta_{O,total}$, with significantly greater uptake at T_{dep} = 700 K. $\theta_{O,surface}$ was determined using surface-sensitive AES measurements and the results in Figure 9D show that for all AO exposures $\theta_{O,total} > \theta_{O,surface}$. Despite the differences in $\theta_{O,total}$, T_{dep} had a much smaller effect on $\theta_{O,surface}$. $\theta_{O,surface}$ ranged from 0.5 ML to slightly less than 0.8 ML; $\theta_{O,surface} < 0.5$ ML were not observed because the AO dosing also exposes the Rh(111) surface to 5×10^{-7} Torr O_2, rapidly saturating the surface with 0.5 ML O [41, 60]. The surface coverages in excess of 0.5 ML could be from other surface structures. $\theta_{O,surface}$ for the $(2\sqrt{3} \times 2\sqrt{3})$ and (2×2)-3O adlayers are 0.66 ML and 0.75 ML, respectively [88]. Both structures have been observed after high-pressure O_2 exposures [82, 88] and fit the AES data in Figure 9D. However, because $\theta_{O,surface}$ was significantly less than 1 ML for all AO exposures, the excess O must have been absorbed into the selvedge of the Rh(111) crystal as subsurface oxygen (O_{sub}), as has been reported previously for high oxygen coverages on and in Rh(111) [18, 60, 66].

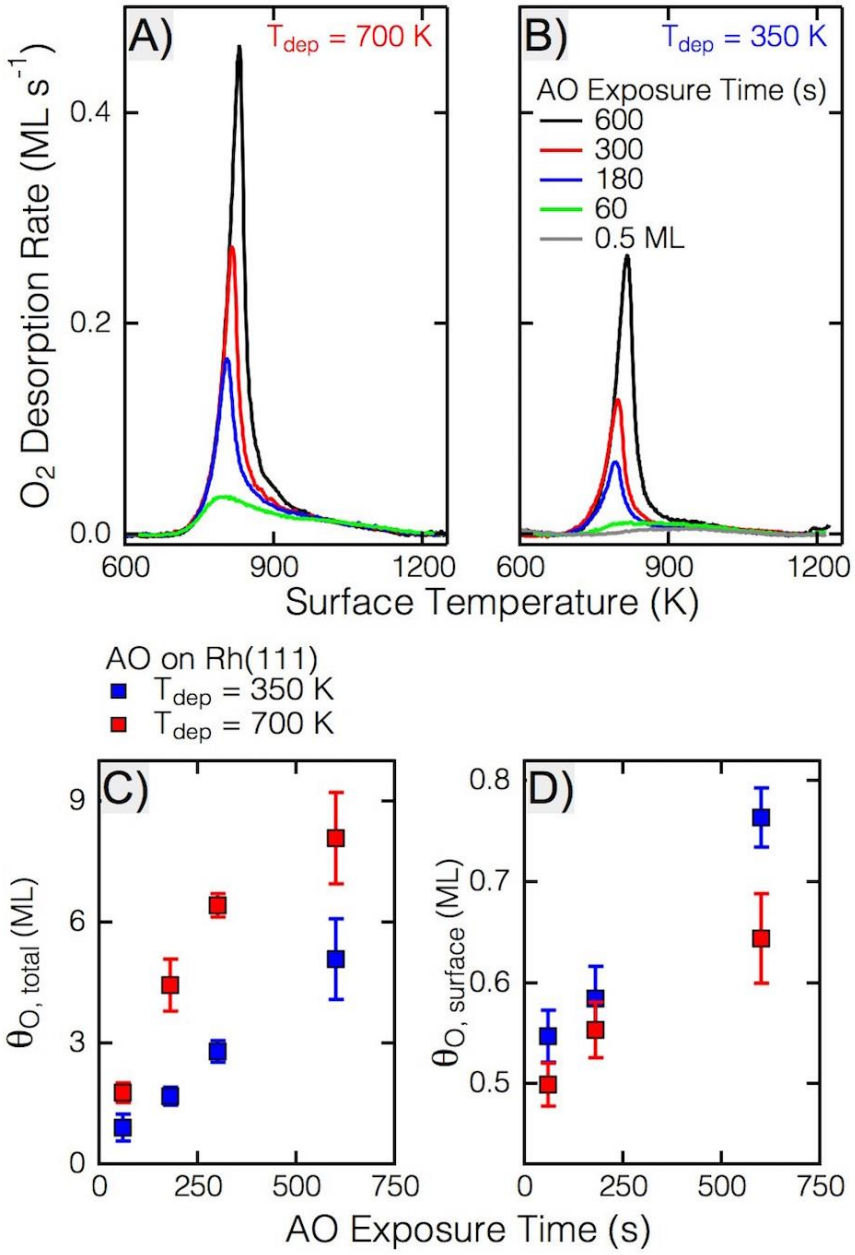

Figure 9. TPD spectra (ramp rate = 3 K s^{-1}) after AO exposures on Rh(111) at A) T_{dep} = 700 K and B) T_{dep} = 350 K. The total oxygen uptake ($\theta_{O,total}$, integrated TPD) vs. AO exposure is shown in C) and the surface coverage ($\theta_{O,surface}$, as determined by AES) is plotted in D). These show only a modest increase in surface coverage despite large increases in total oxygen.

The TPD and AES data show high oxygen abundance, yet modest surface coverage after

AO exposure. Figure 10 depicts how the surface structure changes for several $\theta_{O,total}$ at T_{dep} = 350 K. The STM images and LEED patterns (insets) show the surface changing from the $\theta_{O,total}$ = 0.5 ML (2×1) adlayer structure (Figure 10A) to a distorted (2√3×2√3) R30° with $\theta_{O,total}$ = 0.76 ± 0.06 ML (Figure 10D). As reported in a previous publication[60], the (2×1)-O structure remained predominant despite $\theta_{O,total}$ > 1 ML; these observations were confirmed by the STM and LEED images in Figure 10B. With increasing O uptake, however, the (2√3×2√3) R30° domains grow at the expense of (2×1), as seen in Figure 10C. Finally, at $\theta_{O,total}$ = 2.9 ML (Figure 10D), the LEED showed only a distorted (2√3×2√3) R30° pattern, and likewise the STM images showed the surface covered with extensive domains of (2√3×2√3)R30° intermixed with patches of (2×2)-3O domains. This mixture of surface structures has been previously reported after O_2 exposures at elevated pressure and temperature [88], but has not been shown after AO exposures under UHV compatible conditions and at modest sample temperatures. It is believed that the incorporation of subsurface oxygen (O_{sub}) allows for the formation of the oxide-like structures because, once the oxygen rich domain thickens, the oxygen cannot penetrate to propagate the incorporation of oxygen [17].

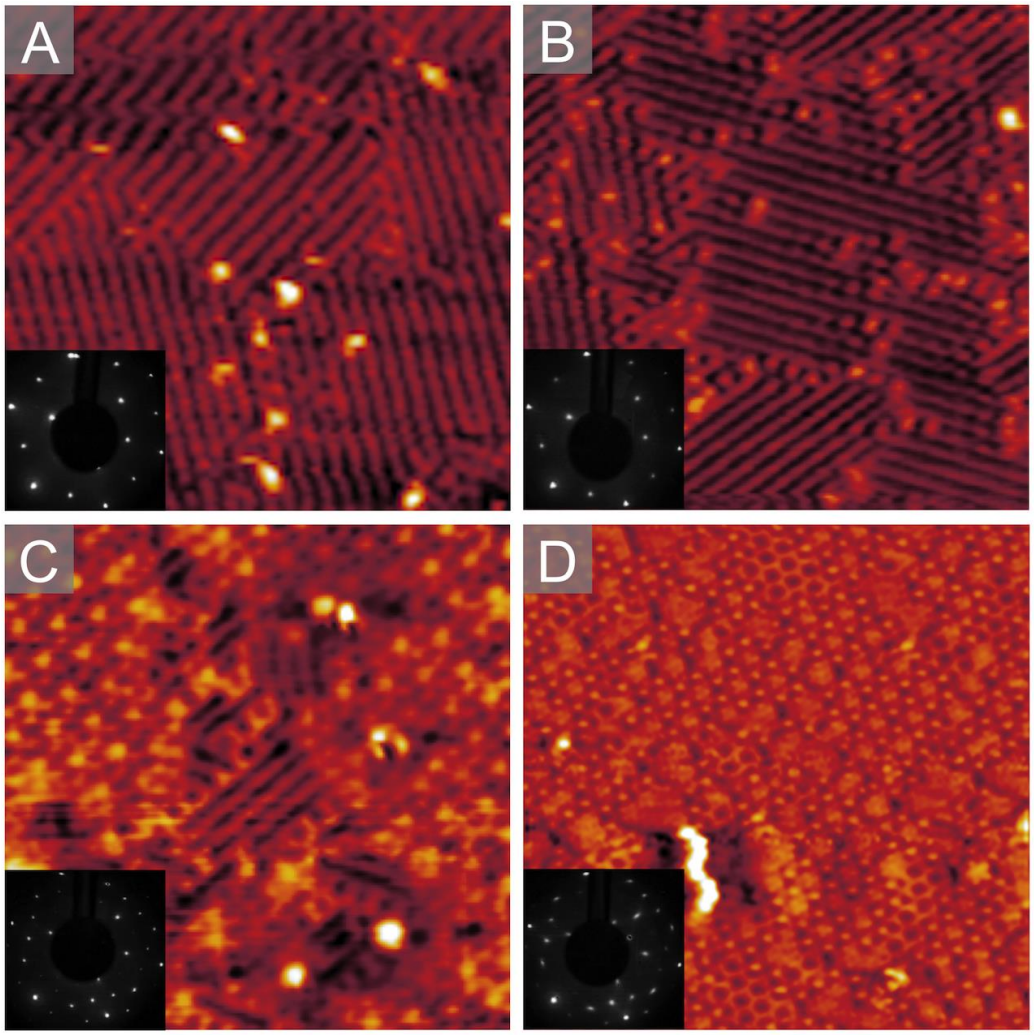

Figure 10. STM images (20 x 20 nm^2) and LEED patterns (insets) of Rh(111) after T_{dep} = 350 K AO/O_2 exposures. $\theta_{O,total}$ = A) 0.5 ML O, B) 0.9 ML O, C) 1.7 ML O, and D) 2.9 ML O. All STM images were taken at 30 K and electron energy was 62 eV for all LEED patterns. STM imaging conditions were A) 0.9 V, 300 pA; B) 20 mV, 288 pA; C) 0.88 V, 200 pA; D) 100 mV, 160 pA

The effect of T_{dep} is evident in that going from 350 K to 700 K, $\theta_{O,total}$ increased dramatically, $\theta_{O,surface}$ decreased slightly, and the O_2 desorption E_a was modestly greater. Taken together, these point to a change in the chemical state of the oxygen on and in Rh(111). The STM images in Figure 11A show the marked difference in the surface structure after exposure at

700 K compared to 350 K. Instead of the intermixed coexistence of $(2\sqrt{3}\times2\sqrt{3})R30°$ and (2×2)-3O structures, the surface was covered in (2×1)-O domains or large hexagonal domains on the top of step edges. These structures were also observed after prolonged 2×10^{-4} mbar O_2 exposures at 800 K [1]. Closer inspection of these hexagonal structures revealed a moiré pattern characteristic of a single (8×8) RhO_2 trilayer oxide on top of a (9×9) Rh(111) substrate [15, 82]. The LEED pattern (inset of Figure 11A) confirms the presence of the surface oxide via spot splitting indicative of the (8×8) oxide periodicity. It is important to note that, although $\theta_{O,total}$ (6.4 ML) is nearly 6 ML above the 0.5 ML coverage of the (2×1) adlayer, this low coverage structure persists on the terraces. Furthermore, the (2×1) domains are much larger than observed for T_{dep} = 350 K, suggesting these to be the stable surface structure at 700 K. The brims of RhO_2 oxide on the top of the step edges account for ≈ 25% of the surface area in the 300 s AO exposure shown in Figure 3A. The fact that they were only observed on the top of step edges, and that every step edge was covered, indicates that defects enhanced their formation.

The stability of the RhO_2 oxide and the (2×1) surface adlayer were further explored by dosing the Rh(111) crystal with AO at T_{dep} = 350 K ($\theta_{O,total}$ = 2.9 ML) and then annealing it to 700 K for 600 s. STM images of the surface after such a treatment are shown in Figure 11B. Rather than a brim of the RhO_2 oxide on top of the step edges, smaller patches of the trilayer were observed along with dendritic features growing from the step edges along the symmetry vectors of the surface on the lower terrace. These dendritic structures are comparable to oxide chains seen during Pt oxidation [85]. Although we are unable to definitively determine the composition of these features, we hypothesize that they are the same RhO_2 as seen for the 700 K

exposure interspersed with dendritic oxide precursors. The fraction of the surface covered by RhO_2 was now about 15%, and longer annealing times had little effect on the structure or coverage of the RhO_2 oxide. The effect of O abundance on the annealed surface was also studied by varying total O uptake. Figure 11C shows STM images of the Rh(111) surface after a 60 s AO exposure ($\theta_{O,total}$ = 0.9 ML) at T_{dep} = 350 K followed by a 600 s anneal at 700 K. Unlike the $\theta_{O,total}$ = 2.9 ML preparation, there were no moiré or dendritic structure present. The surface was instead covered entirely with the (2×1) adlayer, identical to that seen in Figure 10B. With annealing, the (2×1) domains are much larger and well defined. The step edges in Figure 11C are also decorated with 1-D oxide lines similar to those observed on (110) steps [89]. In this case, the surface remains covered in the (2×1) adlayer, and the LEED patterns for both of the annealed surfaces confirm the predominance of the (2×1) surface structure. While Figs. 7B and C show some distortion of the (1×1) and (2×1) LEED pattern respectively, the predominance of these surface structures are clearly evident.

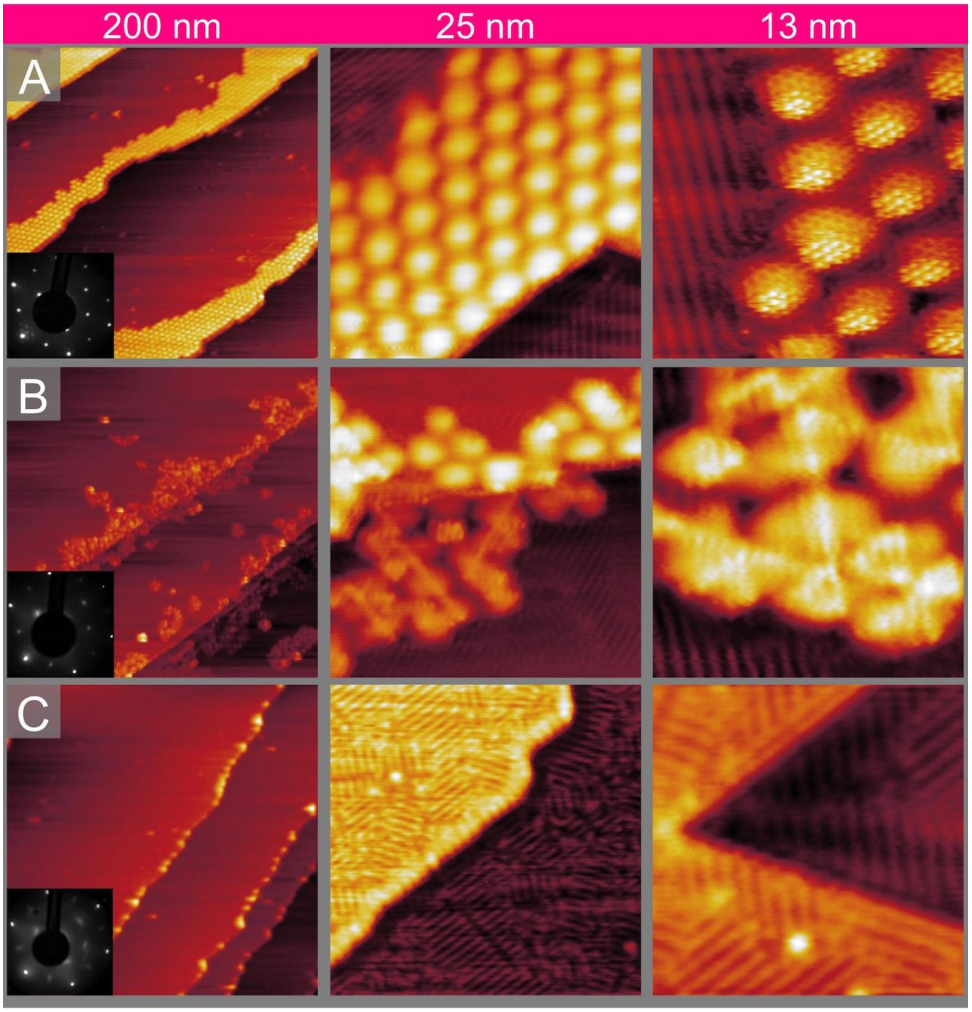

Figure 11. STM images after exposing Rh(111) to AO A) $\theta_{O,total}$ = 6.4 ML at T_{dep} = 700 K.; B) $\theta_{O,total}$ = 2.9 ML at T_{dep} = 350 K followed by 600 s anneal at 700 K; C) $\theta_{O,total}$ = 0.9 ML at T_{dep} = 350 K followed by 600 s anneal at 700 K. Insets are LEED patterns (62 eV) taken after deposition. STM images were obtained at 30 K and conditions were (L to R) (A) 100 mV, 137 pA; 181 mV, 170 pA: 140 mV, 153 pA (B) 50 mV, 400 pA; 70 mV, 410 pA; 50mV, 400 pA C) 20 mV, 200 pA; 20 mV, 150 pA; 20 mV, 150 pA.

Comparison of the post-annealing structures from $\theta_{O,total}$ = 2.9 ML and 0.9 ML show the effect of O_{sub} on the presence of the surface oxide. For both, $\theta_{O,surface}$ was the same, but the amount of O_{sub} differed, $\theta_{O,sub} \approx$ 2.3 ML and 0.3 ML, respectively. Therefore, any surface differences can be attributed to the amount of O_{sub} present before annealing. The fact that no appreciable RhO_2 was observed unless > 1 ML O_{sub} was available suggests that the RhO_2 surface

oxide forms from O_{sub}, and the surface oxide will only form once enough O_{sub} is present in the Rh crystal.

Another factor is the difference in O uptake for the two temperatures. For all exposures, $\theta_{O,total}$ was roughly double for T_{dep} = 700 K compared to T_{dep} = 350 K. This was likely because the O atoms at 350 K did not have enough energy to diffuse more than 4-5 layers deep into the Rh selvedge, which filled more quickly, as evidenced by the quicker uptake rollover seen in Figure 9C. Alternatively, at 700 K, the O atoms in the selvedge were much more mobile, and penetrated farther into the surface. This resulted in a higher concentration of O in the selvedge and a localized oxygen rich environment. When looking at the phases in the oxygen rich regime, the oxide, RhO_2, is the thermodynamically preferred structure [90-91]. Extended AO exposure resulted in significant oxygen absorption into the subsurface region once the surface saturates at 0.65 ML, this agrees with previous work studying high O coverage structures[1, 90, 92]. We are presently studying oxidation reactions on the different surface phases to determine how their chemistry may differ.

In summary, high coverage O/Rh surface structures were prepared using AO dosing. Preparation conditions were developed to investigate the thermodynamic stability of the resulting O adlayers and oxide structures, as well as the surface conditions necessary to form the thin film surface oxide RhO_2. At 700 K, the (2×1) adlayer was stable regardless of O_{sub} concentration. By tuning the amount of subsurface oxygen present in the system, as well as the Rh(111) temperature during AO deposition or annealing, we were able to selectively form the surface oxide as well as a variety of O adlayers. When the concentration of O_{sub} was increased, and the sample was prepared at or annealed at 700 K, we were able to generate the surface oxide and a

dendritic oxide precursor without the presence of bulk oxide. This illustrated the thermodynamic stability of the (2×1) adlayer, as well as the formation of RhO_2 surface oxide when sufficient O_{sub} was present. Fine control of the deposition conditions allowed for a clear connection between subsurface oxygen and surface defects and the formation of the catalytically important RhO_2 surface oxide.

CHAPTER FOUR

LOW TEMPERATURE CO OXIDATION ON OXIDIZED RH(111)

The arrangement and interaction of atoms on catalytic surfaces directly influences the resultant products formed. For this reason, a driving goal in the study of heterogeneously catalyzed reactions using surface science techniques has been to understand the atomistic mechanism of various heterogeneously catalyzed reactions. Traditional surface science techniques, however, require ultra-high vacuum (UHV) conditions that can result in fundamentally different surface structures and chemical mechanisms from those seen on catalysts under actual catalytic conditions[21].

The discrepancy between UHV studies and actual catalysis, referred to as the "pressure gap", has inspired innovations in the field of surface science to prepare more catalytically representative surfaces for thorough study[23-24, 30, 93]. One such development has been the ability to create surfaces present under actual catalysis conditions for study in UHV surface science studies. By utilizing high pressure and temperature O_2 preparations[49], atomic oxygen (AO) plasmas[85], and gas phase AO exposures[48], catalytically relevant oxidized surfaces can be prepared that were previously unobtainable with UHV compatible preparation techniques. In generating highly oxidized surfaces, it has been shown that oxide surfaces, rather than only metallic surfaces with an oxygen adlayer, are extremely relevant for catalytic activity[5, 33-34]. On Rh, the surface oxide (RhO_2) has been suggested as the catalytically relevant phase for CO oxidation, but there is debate as to the extent the surface oxide actually plays.

While some work shows the surface oxide as necessary for high CO_2 yield from CO oxidation on Rh surfaces[10], other shows that the metallic Rh surface with adsorbed oxygen (O_{ad}) is the truly active catalyst[10, 94-95].

In this work, we have prepared well characterized oxidized Rh(111) surfaces containing the 0.5 monolayer (ML) (2×1)-O adlayer, RhO_2, and subsurface oxygen (O_{sub})[48] to study the active sites for CO oxidation using temperature programmed desorption (TPD) and scanning tunneling microscopy (STM). By utilizing TPD to track residual oxygen (O_{res}) desorption and CO_2 yield following CO exposure, we compared the reactivity of the saturated (2×1)-O surface with the RhO_2 surface. STM was then used to identify the exact reaction site on the oxidized Rh(111) surface. By combining TPD data that shows the relative reactivity of the distinct oxidized surfaces and STM data that shows atomic scale detail of surface reactivity, we are able to identify the active surface phase, as well as begin to understand factors that enhance CO oxidation on Rh catalysts.

Experiments were performed in an ultrahigh-vacuum (UHV) apparatus comprised of a preparation chamber and a scanning tunneling microscope (UHV-STM, RHK Technology, Troy, MI) chamber described previously[60]. The Pan-style STM is cooled using a closed-cycle He cryostat, and has a base temperature of approximately 12 K. The Rh(111) crystal (Surface Preparation Laboratory, Zaandam, NL) was mounted on a Ta sample holder (McAllister Technical Services, Coeur d'Alene, ID) with a type-K thermocouple. The Rh(111) sample was cleaned with repeated cycles of Ar^+ sputtering and annealing at 1300 K. The cleanliness was verified by Auger electron spectroscopy (AES), a clean (1×1) LEED pattern, and STM imaging to obtain the Rh(111) atomic lattice. Atomic oxygen was generated using a hot Ir filament as

previously reported[35, 60]. TPD spectra were recorded with a UTI 100c quadrupole mass spectrometer controlled by a homebuilt labVIEW program. Rh(111) exposed to O_2 at 350 K results in the saturated (2×1)-O 0.5 ML O_{ad} surface; the integral of the O_2 spectra was used to

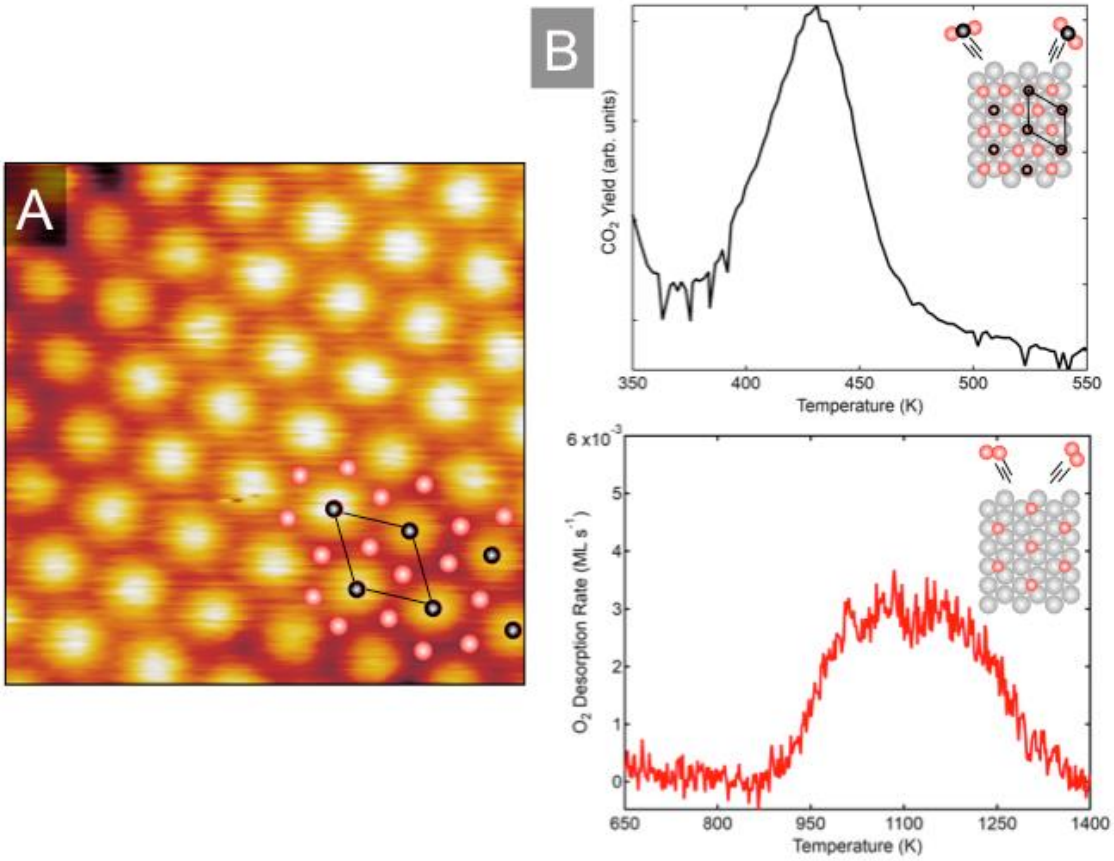

Figure 12. A) STM image (5 × 5 nm^2) of (2×2)-O+CO, 1.02 V, 0.69 nA B) Representative TPD spectra of CO_2 yield (left) and O_{res} (right) following O_2 exposure at T_{dep} = 350 K and CO exposure at T_{dep} = 300 K.

calibrate subsequent O_2 TPD spectra. The oxidized Rh(111) surface was held at either 300 K or 200 K during CO exposure. For TPD experiments following CO exposure, the crystal was cooled to 100 K. TPD spectra from 100-600 K used a ramp rate of 4 K s^{-1} and tracked evolution of CO_2. Following this initial TPD experiment, the sample was cooled to 400 K. TPD spectra from 400-

1400K used a ramp rate of 3 K s^{-1}; and residual oxygen (O_{res}) remaining on the surface following CO oxidation was tracked. All STM images were taken at 30 K. As previously mentioned, there was neither background gas accumulation nor surface degradation following prolonged STM experiments[87].

Much work has been done to further the understanding of CO oxidation on the (2×1)-O/Rh(111) surface[42, 96-98]. CO adsorbs to the (2×1)-O surface resulting in (2×2)-O+CO overlayer[99]. This is supported experimentally and theoretically for the Rh(111) surface, and an STM image of the (2×2)-O+CO surface can be seen in Figure 12A. Additionally, a representative TPD spectra following CO exposure at 300 K can be seen in Figure 12B. TPD experiments were performed following a 300 K and 100 K CO exposure to (2×1)-O/Rh(111), and the CO_2 yield and O_{res} were similar for the two temperatures. This supports previous claims that the O+CO overlayer is stable at room temperature and lower[39]. The CO_2 TPD in Figure 12B also shows that the maximum CO_2 desorption occurs at 425 K.

Previous work has shown in detail that Rh(111) can be oxidized using AO to selectively form RhO_2, (2×1)-O, and O_{sub}[48]. After preparing an oxidized Rh(111) surface with 3 ML equivalence of oxygen, CO exposures were conducted at 300 K. Since CO exposures at 100 and 300 K were identical for the (2×1)-O surface, and the maximum desorption temperature for CO_2 was determined to be 425 K, CO exposures at 300 K should have been low enough for the O+CO adlayer to be stable on the RhO_2 surface preparation. The surface was held at 700 K and exposed to AO generating an uptake of 3 ML oxygen. Following the preparation of the oxidized sample, the surface was exposed to CO at 300 K for various exposure lengths. Due to our TPDs not discriminating against background gas in the chamber, initial oxidation behavior was

analyzed by looking at the amount of O_{res}. If the amount of O_{res} corresponds to the oxygen remaining after CO has oxidized the other oxygen species on the surface, the amount of O_{res} can serve as a qualitative mark for surface reactivity.

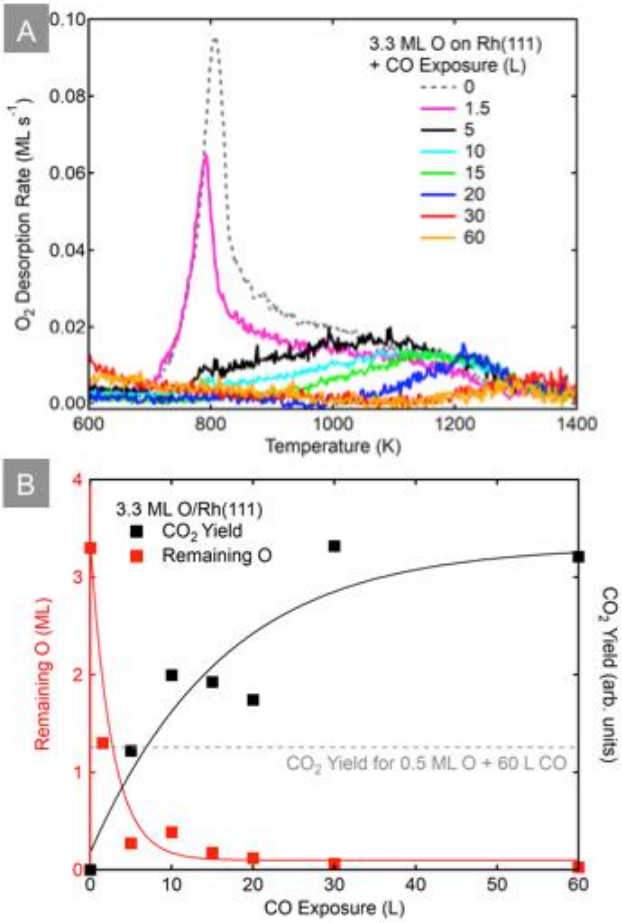

Figure 13. A) TPD spectra of O_{res} following AO exposures at T_{dep} = 700 K and CO exposures at T_{dep} = 300 K. B) Integrated TPD area of O_{res} and CO_2 yield.

While we started with ~ 3 ML O present, after a 1.5 L CO exposure, the intensity of the O_{res} peak has decreased disproportionally relative to the length of the CO exposure as seen in Figure 13A. As CO exposure is increased, we can see that the O_{res} amount continues to decrease until it is difficult to detect above the gas background of the chamber.

When we compare the O_{res} against the CO_2 yield, as seen in Figure 13B, we can see that the O_{res} decreases rapidly while there is a simultaneous roll over in the amount of CO_2 detected. Interestingly, the amount of CO_2 detected is roughly double that detected from the (2×1)-O surface, supporting the assignment that RhO_2 is more catalytically active for CO oxidation due to the increased CO_2 yield[10, 28, 34, 49]. Additionally, while there is a continuous decrease in the amount of O_{res}, the CO_2 yield is constant. If 3 ML equivalence of oxygen is to be reacted from a surface, it would be suspected that a comparable amount of product (CO_2) be detected to correlate to the consumed oxygen. Previous work has suggested that when CO oxidation is taking place in an oxygen rich environment, the activation energy for oxidation is lowered[100]. In addition, the work function of Rh is altered by the introduction of oxygen into the metal, as adsorbed and absorbed oxygen[101]. For these reasons, there could be a lower temperature oxidation reaction occurring due to the oxygen rich surface and lowered activation energy.

To determine if there is, indeed, low temperature oxidation occurring, we need to be able to track the surface structure evolution, since there is no way to detect CO_2 that may be forming during the CO exposure or surface cool to T_1 for the TPD experiments. In order to achieve this

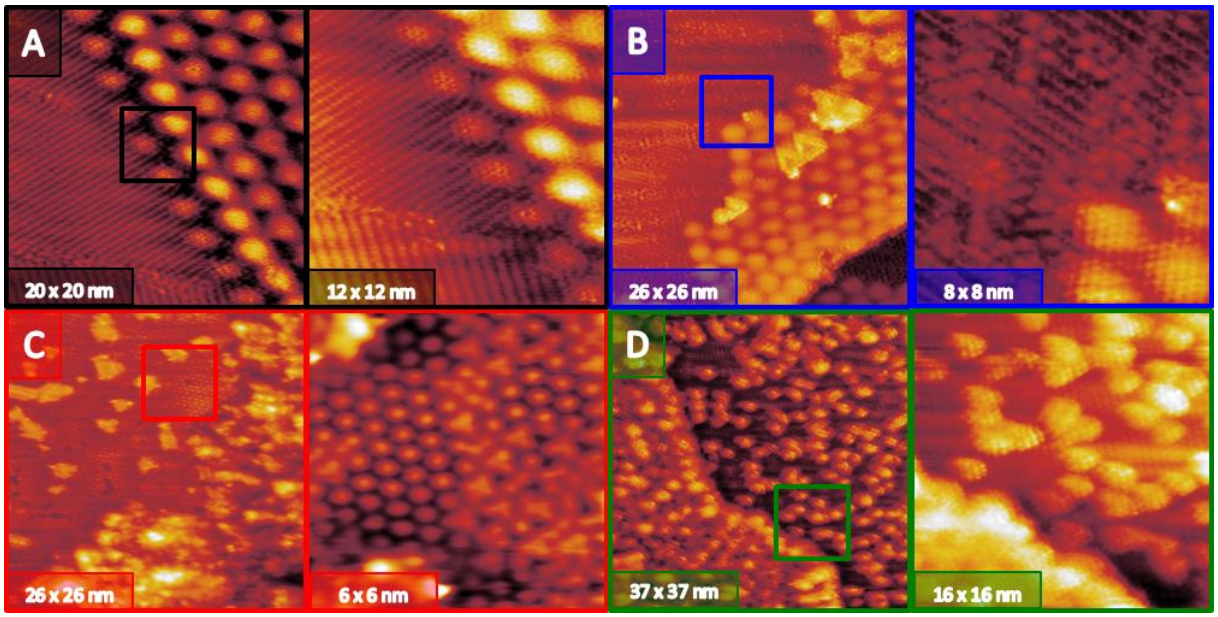

Figure 14. STM images after T_{dep} = 700 K AO exposures and T_{dep} = 300 K CO exposures for various CO exposures. A) Bare RhO_2 243 mV, 301 pA; B) 1.5 L CO, -1.01 V, -0.87 nA, inset 414 mV, 260 pA; C) 60 L CO, 0.88 V, 230 pA, inset 1.26 V, 0.81 nA; D) 120 L CO, -280 mV, -0.96 nA, inset -280 mV, -0.96 nA.

reaction snapshot, we utilized low temperature STM imaging to effectively freeze any surface reconstruction or evolution occurring during CO exposure. The CO exposures were done at 300 and 200 K to see if the same surface structure evolution occurred. As seen in Figure 14B, after a 1.5 L CO exposure at 300 K, there are adsorbates on the (2×1) O adlayer as well as aggregation along the RhO_2 moiré/(2×1) boundary. Additionally, there are triangular features forming on the moiré pattern. These triangular features are not seen on the bare RhO_2 surface, as shown in Figure 14A, suggesting that the new features are the result of CO adsorption on the surface

oxide. The step edge of the moiré also has evidence of adsorbates, indicating that CO adsorbs preferentially to domain boundaries and defect sites as suggested in previous work[10]. Increasing CO exposure to 60 L, when very little O_{res} is detected in TPD experiments (Figure 13A), a more drastic surface evolution is seen in Figure 14C. The domain near the step edge that had surface oxide is now completely consumed by disordered clusters and the terrace is covered in a (2×2)-O+CO adlayer, consistent with CO adsorption on the (2×1)-O adlayer. The terrace is also decorated with bright islands. Upon closer inspection of the terrace, the corresponding inset of Figure 14C, there are triangle-like clusters intermixed with the (2×2)-O+CO adlayer. These triangular clusters agree well with the structure seen for CO adsorbed directly onto Rh(111)[102]. The only way for bare Rh to be present following AO exposure is if CO is being oxidized during the CO exposure at 300 K, thus allowing for CO to adsorb directly to the metal surface. Since CO binds more strongly to the Rh surface than CO_2, it is reasonable for the CO molecule to remain adsorbed on the surface at 300 K. Increasing the exposure to 120 L, shown in Figure 14D, the surface is completely covered in bright clusters and the (2×2)-O+CO adlayer. There is no longer any evidence of surface oxide, and the terraces have clusters regardless of the site distance from a step edge or defect site. Such drastic reconstruction of the oxidized surface following CO exposure is consistent with reconstruction seen following CO oxidation on Rh surfaces, and suggests that the surface must be catalyzing CO oxidation below reaction temperatures.

While 300 K is below the reaction temperature needed for CO oxidation to occur on the oxidized Rh surface, we wanted to confirm that the surface evolution observed is solely due to

low temperature CO oxidation. To do so, we repeated CO exposure to the RhO_2 surface at 200 K, significantly below the reaction temperature for CO oxidation. The surface of the 200 K

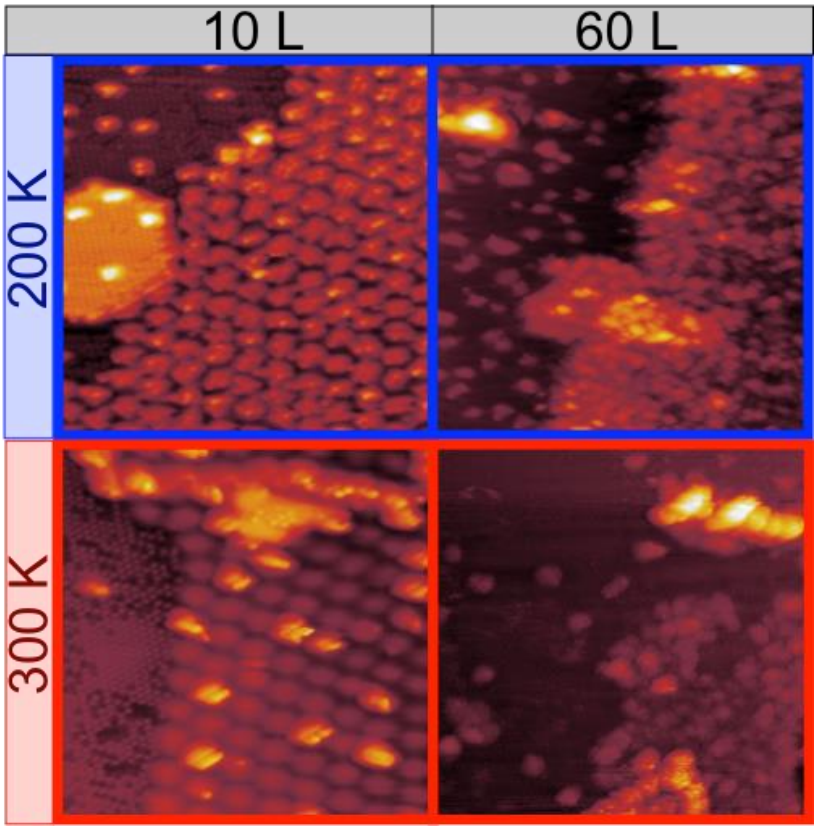

Figure 15. STM images CO exposure at either T_{dep} = 200 or 300 K. T_{dep} = 200 K images 25 × 25 nm^2. T_{dep} = 300 K images 45 × 45 nm^2. T_{dep} = 200 K, 10 L CO -1.22 V, -0.92 nA; T_{dep} = 200 K, 60 L CO -0.85 V, -0.70 nA; T_{dep} = 300 K, 10 L CO 2.23 V, 90 pA; T_{dep} = 300 K, 60 L CO 1.06 V, 350 pA

CO exposure was then directly compared to identical CO exposures done at 300 K, as shown in Figure 15. The surface evolution of the 200 K preparation is identical to the 300 K preparation. For both of the 10 L exposures in Figure 15, the moiré pattern is interrupted with linear decorations, the terraces are covered in the (2×2)-O+CO adlayer, and in the 200 K CO exposure, an island of moiré is completely covered in the (2×2)-O+CO adlayer. For the 60 L CO exposure

in Figure 15, both surfaces have had the surface oxide completely consumed, and islands are beginning to form on the terrace as well. Since both temperatures are evolving in identical manners, it is likely that low temperature CO oxidation is occurring.

In this work, we have shown evidence of low temperature CO oxidation occurring on a Rh(111) crystal that has been oxidized using AO to form the (2×1)-O adlayer, RhO_2 surface oxide, and O_{sub}. While the exact mechanism for low temperature CO oxidation is not currently known, the CO oxidation begins at domain boundaries and defect sites on the crystal and surface oxide. We have shown, with molecular resolution, that the surface oxide is entirely consumed during CO oxidation at 300 and 200 K, confirming the important role of surface oxide in catalytic oxidation.

CHAPTER FIVE

CONCLUSIONS AND FUTURE WORK

In this dissertation work, gas phase atomic oxygen (AO) has been used to prepare relevant high coverage adlayers and surface oxides on catalytically relevant single metal crystals.

First, the effects of defect density and catalyst material on the stability of subsurface oxygen (O_{sub}) was studied by comparing the structural evolution and oxygen uptake of Pt(553) and Rh(111) following AO exposure on Rh(111)[55]. It was shown that the stability of O_{sub} was not enhanced on Pt(553) relative to Pt(111) despite the high defect density of Pt(553). On Rh(111), however, O_{sub} readily formed, resulting in a mixture of high coverage oxygen adlayers. This study supported the observation that certain metals more readily stabilize and form O_{sub}, and the addition of defect sites does not drastically alter the inherent affinity for O_{sub} formation of a metal.

Second, using traditional ultra-high vacuum (UHV) surface science techniques, preparation conditions were carefully controlled to allow for the selective formation of various oxygen phases on Rh(111)[48]. By varying the temperature of the substrate during AO exposure, either high coverage oxygen adlayers or the Rh surface oxide, RhO_2, formed. Additionally, annealing experiments demonstrated the importance of O_{sub} population in the stability and formation of RhO_2. The ability to selectively form various catalytically relevant phases using UHV preparation methods allows for atomistic structural information that is difficult to

obtain when using elevated temperature and high pressure oxidizing conditions.

Finally, utilizing the preparation methods to generate RhO_2 on Rh(111), the active site for CO oxidation was investigated. During the course of this study, it was shown that CO oxidation occurs at significantly lower temperatures in the presence of RhO_2. Additionally, atomically resolved structural information reveals that CO preferentially adsorbs to defect sites and grain boundaries at low CO coverages on the oxidized Rh surface, and as coverage increases, the CO completely consumes the surface oxide. The consumption of CO during low temperature CO oxidation was observed for temperatures as low as 200 K.

In order to fully characterize the oxygen speciation present on Rh(111) following exposure to AO at various substrate temperatures, high-resolution X-ray photoelectron spectroscopy (HR XPS) will be used to probe the unique chemical states of adsorbed oxygen and the Rh surface as various surface structures evolve. This will allow for a detailed understanding of the chemical properties of the oxygen phases present on Rh(111), giving insight into their potential catalytic activity.

While previous work in the Killelea lab has focused on O_{sub} characterization on Ag(111)[103], reactivity studies have not been carried out on Ag(111). Future work will look to probe unique reactivity of various oxygen phases on Ag(111) and Ag (110), and determine the structural evolution of the oxidized Ag surface following oxidation reactions. It is of interest to understand reactivity behavior and structural evolution of Pd surfaces, and similar reactivity studies will also be done on Pd single crystals in the future.

REFERENCE LIST

1. Gustafson, J.; Mikkelsen, A.; Borg, M.; Lundgren, E.; Kohler, L.; Kresse, G.; Schmid, M.; Varga, P.; Yuhara, J.; Torrelles, X.; Quiros, C.; Andersen, J. N., Self-Limited Growth of a Thin Oxide Layer on Rh(111). *Physical Review Letters* **2004,** *92* (12), 126102.

2. Cuena, B. R., Metal Nanoparticle Catalysts Begin to Shape-up. *Acc. Chem. Res.* **2012,** *46*, 1682-1691.

3. Landmarks, A. C. S. N. H. C. The Houdry Process for Catalytic Cracking. http://www.acs.org/content/acs/en/education/whatischemistry/landmarks/houdry.html (accessed February).

4. Weaver, J. F., Surface Chemistry of Late Transition Metal Oxides. *Chemical Reviews* **2013,** *113* (6), 4164-4215.

5. Freund, H. J., The Surface Science of Catalysis and More, Using Ultrathin Oxide Films as Templates: A Perspective. *Journal of the American Chemical Society* **2016,** *138* (29), 8985-8996.

6. Campbell, C. T., Atomic and molecular oxygen adsorption on Ag(111). *Surface Science* **1985,** *157*, 43-60.

7. Rovida, G.; Pratesi, F.; Magliett.M; Ferroni, E., Chemisorption of Oxygen on Silver (111) Surface. *Surface Science* **1974,** *43* (1), 230-256.

8. Bao, X.; Barth, J. V.; Lehmpfuhl, G.; Schuster, R.; Uchida, Y.; Schlogl, R.; Ertl, G., Oxygen-Induced Restructuring of Ag(111). *Surface Science* **1993,** *284* (1-2), 14-22.

9. Schnadt, J.; Knudsen, J.; Hu, X. L.; Michaelides, A.; Vang, R. T.; Reuter, K.; Li, Z.; Laegsgaard, E.; Scheffler, M.; Besenbacher, F., Experimental and theoretical study of oxygen adsorption structures on Ag(111). *Physical Review B* **2009,** *80* (7), 075424.

10. Gustafson, J.; Westerstrom, R.; Balmes, O.; Resta, A.; van Rijn, R.; Torrelles, X.; Herbschleb, C. T.; Frenken, J. W. M.; Lundgren, E., Catalytic Activity of the Rh Surface Oxide: CO Oxidation over Rh(111) under Realistic Conditions. *Journal of Physical Chemistry C* **2010,** *114* (10), 4580-4583.

11. Jones, T. E.; Rocha, T. C. R.; Knop-Gericke, A.; Stampfl, C.; Schlogl, R.; Piccinin, S., Thermodynamic and Spectroscopic Properties of Oxygen on Silver under an Oxygen Atmosphere. *Physical Chemistry Chemical Physics* **2015,** *17* (14), 9288-9312.

12. Li, W. X.; Stampfl, C.; Scheffler, M., Subsurface Oxygen and Surface Oxide Formation at Ag(111): A Density-Functional Theory Investigation. *Physical Review B* **2003,** *67* (4), 045408.

13. Verwey, E. J. W.; de Boer, J. H., Surface oxide films. *Recl. Trav. Chim. Pays-Bas* **1936,** *55* (8), 0165-0513.

14. Gustafson, J.; Mikkelsen, A.; Borg, A.; Andersen, J. N.; Lundgren, E.; Klein, C.; Hofer, W.; Schmid, M.; Varga, P.; Kohler, L.; Kresse, G.; Kasper, N.; Stierle, A.; Dosch, H., Structure of a thin oxide film on Rh(100). *Physical Review B* **2005,** *71* (11), 115442.

15. Blomberg, S.; Lundgren, E.; Westerstrom, R.; Erdogan, E.; Martin, N. M.; Mikkelsen, A.; Andersen, J. N.; Mittendorfer, F.; Gustafson, J., Structure of the Rh_2O_3(0001) Surface. *Surface Science* **2012,** *606* (17-18), 1416-1421.

16. Greeley, J.; Mavrikakis, M., On the role of subsurface oxygen and ethylenedioxy in ethylene epoxidation on silver. *Journal of Physical Chemistry C* **2007,** *111* (22), 7992-7999.

17. Todorova, M.; Li, W. X.; Ganduglia-Pirovano, M. V.; Stampfl, C.; Reuter, K.; Scheffler, M., Role of Subsurface Oxygen in Oxide Formation at Transition Metal Surfaces. *Physical Review Letters* **2002,** *89* (9), 096103.

18. Gibson, K. D.; Killelea, D. R.; Sibener, S. J., Comparison of the Surface and Subsurface Oxygen Reactivity and Dynamics with CO Adsorbed on Rh(111). *Journal of Physical Chemistry C* **2014,** *118* (27), 14977-14982.

19. Ertl, G., Reactions at surfaces: From atoms to complexity (Nobel lecture). *Angewandte Chemie-International Edition* **2008,** *47* (19), 3524-3535.

20. Campbell, C. T., Atomic and Molecular-Oxygen Adsorption on Ag(111). *Surface Science* **1985,** *157* (1), 43-60.

21. Freund, H.-J.; Kuhlenbeck, H.; Libuda, J.; Rupprechter, G.; Bäumer, M.; Hamannm, H., Bridging the pressure and materials gaps between catalysis and surface science: clean and modified oxide surfaces. *Topics in Catalysis* **2001,** *15*, 201-209.

22. Rider, K. B.; Hwang, K. S.; Salmeron, M.; Somorjai, G. A., High-pressure (1 Torr) scanning tunneling microscopy (STM) study of the coadsorption and exchange of CO and NO on the Rh(111) crystal face. *Journal of the American Chemical Society* **2002,** *124* (19), 5588-5593.

23. Salmeron, M.; Schlogl, R., Ambient pressure photoelectron spectroscopy: A new tool for surface science and nanotechnology. *Surface Science Reports* **2008,** *63* (4), 169-199.

24. Herbschleb, C. T.; van der Tuijn, P. C.; Roobol, S. B.; Navarro, V.; Bakker, J. W.; Liu, Q.; Stoltz, D.; Canas-Ventura, M. E.; Verdoes, G.; van Spronsen, M. A.; Bergman, M.; Crama, L.; Taminiau, I.; Ofitserov, A.; van Baarle, G. J. C.; Frenken, J. W. M., The ReactorSTM: Atomically resolved scanning tunneling microscopy under high-pressure, high-temperature catalytic reaction conditions. *Review of Scientific Instruments* **2014,** *85* (8).

25. van Rijn, R.; Balmes, O.; Resta, A.; Wermeille, D.; Westerstrom, R.; Gustafson, J.; Felici, R.; Lundgren, E.; Frenken, J. W. M., Surface structure and reactivity of Pd(100) during CO oxidation near ambient pressures. *Physical Chemistry Chemical Physics* **2011,** *13* (29), 13167-13171.

26. Rocha, T. C. R.; Oestereich, A.; Demidov, D. V.; Havecker, M.; Zafeiratos, S.; Weinberg, G.; Bukhtiyarov, V. I.; Knop-Gericke, A.; Schlogl, R., The silver-oxygen system in catalysis: new insights by near ambient pressure X-ray photoelectron spectroscopy. *Physical Chemistry Chemical Physics* **2012,** *14* (13), 4554-4564.

27. Tao, F., Design of an in-house ambient pressure AP-XPS using a bench-top X-ray source and the surface chemistry of ceria under reaction conditions. *Chemical Communications* **2012,** *48* (32), 3812-3814.

28. Gustafson, J.; Blomberg, S.; Martin, N. M.; Fernandes, V.; Borg, A.; Liu, Z.; Chang, R.; Lundgren, E., A high pressure x-ray photoelectron spectroscopy study of CO oxidation over Rh(100). *J. Phys. Condens. Matter* **2014,** *26*, 055003-05009.

29. Blomberg, S.; Westerstrom, R.; Martin, N. M.; Lundgren, E.; Andersen, J. N.; Messing, M. E.; Gustafson, J., A high-pressure X-ray photoelectron spectroscopy study of oxidation and reduction of Rh(100) and Rh nanoparticles. *Surface Science* **2014,** *628*, 153-158.

30. Montano, M.; Tang, D. C.; Somorjai, G. A., Scanning tunneling microscopy (STM) at high pressures. Adsorption and catalytic reaction studies on platinum and rhodium single crystal surfaces. *Catalysis Letters* **2006,** *107* (3-4), 131-141.

31. Somorjai, G. A.; Park, J. Y., Evolution of the Surface Science of Catalysis from Single Crystals to Metal Nanoparticles Under Pressure. *Journal of Chemical Physics* **2008,** *128* (18), 182504.

32. Li, L.; Yang, J. C., Complex oxide structures formed by oxidation of Ag(100) and Ag(111) by hyperthermal atomic oxygen. *Materials at High Temperatures* **2003,** *20* (4), 601-606.

33. Lundgren, E.; Gustafson, J.; Resta, A.; Weissenrieder, J.; Mikkelsen, A.; Andersen, J. N.; Kohler, L.; Kresse, G.; Klikovits, J.; Biederman, A.; Schmid, M.; Varga, P., The Surface Oxide as a Source of Oxygen on Rh(111). *Journal of Electron Spectroscopy and Related Phenomena* **2005,** *144*, 367-372.
34. Kim, S. M.; Qadir, K.; Seo, B.; Jeong, H. Y.; Joo, S. H.; Terasaki, O.; Park, J. Y., Nature of Rh Oxide on Rh Nanoparticles and Its Effect on the Catalytic Activity of CO Oxidation. *Catalysis Letters* **2013,** *143* (11), 1153-1161.

35. Derouin, J.; Farber, R. G.; Heslop, S. L.; Killelea, D. R., Formation of Surface Oxides and Ag_2O Thin Films with Atomic Oxygen on Ag(111). *Surface Science* **2015,** *641*, L1-4.

36. Grass, M. E.; Zhang, Y.; Butcher, D. R.; Park, J. Y.; Li, Y.; Bluhm, H.; Bratlie, K. M.; Zhang, T.; Somorjai, G. A., A Reactive Oxide Overlayer on Rhodium Nanoparticles during CO Oxidation and Its Size Dependence Studied by In Situ Ambient-Pressure X-ray Photoelectron Spectroscopy. *Angewandte Chemie-International Edition* **2008,** *47* (46), 8893-6.

37. Horn, R.; Williams, K. A.; Degenstein, N. J.; Schmidt, L. D., Syngas by catalytic partial oxidation of methane on rhodium: Mechanistic conclusions from spatially resolved measurements and numerical simulations. *Journal of Catalysis* **2006,** *242* (1), 92-102.

38. Renzas, J. R.; Zhang, Y. W., Rhodium nanoparticle shape dependence in the reduction of NO by CO. *Catal. Lett.* **2009,** *132*, 317-322.

39. Schwegmann, S.; Over, H.; DeRenzi, V.; Ertl, G., The atomic geometry of the O and CO+O phases on Rh(111). *Surface Science* **1997,** *375* (1), 91-106.

40. Marchini, S.; Sachs, C.; Wintterlin, J., STM investigation of the (2x2)O and (2x1)O structures on Rh(111). *Surface Science* **2005,** *592* (1-3), 58-64.

41. Thiel, P. A.; Yates, J. T.; Weinberg, W. H., Interaction of Oxygen With the Rh(111) Surface. *Surface Science* **1979,** *82* (1), 22-44.

42. Matsushima, T.; Matsui, T.; Hashimoto, M., Kinetic studies on the CO oxidation on a Rh(111) surface by means of angle-resolved thermal desorption. *Journal of Chemical Physics* **1984,** *81*, 5151.

43. Xu, H.; Ng, K. Y. S., STM study of oxygen on Rh(111). *Surface Science* **1997,** *375* (2-3), 161-170.

44. Sibener, S. J.; Peterlinz, K. A.; Sibener, S. J., Absorption, Adsorption, and Desorption Studies of the Oxygen/Rh(111) System Using O2, NO, and NO2. *Journal of Physical Chemistry* **1995,** *99* (9), 2817-2825.

45. Grant, J.; Haas, T., A Study of Ru(0001) and Rh(111) Surfaces Using LEED and Auger Electron Spectroscopy. *Surface Science* **1970,** *21*, 76-85

46. Castner, D.; Sexton, B.; Somorjai, G., LEED and Thermal Desorption Studies of Small Molecules (H2, O2, CO, CO2, NO,C2H4, C2H2, and C) Chemisorbed on Rhodium (111) and (100). *Surface Science* **1978,** *71*, 519-540.

47. Wong, K. C.; Liu, W.; Mitchell, K. A. R., LEED crystallographic analysis for the Rh(111)-(2x1)-O surface structure. *Surface Science* **1996,** *360* (1-3), 137-143.

48. Farber, R. G.; Turano, M. E.; Oskorep, E. C. N.; Wands, N. T.; Iski, E. V.; Killelea, D. R., The Quest for Stability: Structural dependence of Rh(111) on oxygen coverage at elevated temperature. *The Journal of Physcial Chemistry C* **2017,** *121* (19), 10470-10475.

49. Gustafson, J.; Westerström, R.; Mikkelsen, A.; Torrelles, X.; Balmes, O.; Bovet, N.; Andersen, J. N.; Baddeley, C. J.; Lundgren, E., Sensitivity of Catalysis to Surface Structure: The Example of CO Oxidation on Rh Under Realistic Conditions *Physical Review B* **2008,** *78* (4), 045423.

50. Musselwhite, N.; Somorjai, G. A., Investigations of Structure Sensitivity in Heterogeneous Catalysis: From Single Crystals to Monodisperse Nanoparticles. *Topics in Catalysis* **2013,** *56* (15-17), 1277-1283.

51. Wachs, I. E., Extending surface science studies to industrial reaction conditions: mechanism and kinetics of methanol oxidation over silver surfaces. *Surface Science* **2003,** *544* (1), 1-4.

52. Kan, H. H.; Weaver, J. F., Mechanism of PdO Thin Film Formation During the Oxidation of Pd(111). *Surface Science* **2009,** *603* (17), 2671-2682.

53. Weaver, J. F.; Chen, J.-J.; Gerrard, A. L., Oxidation of Pt(111) by Gas-Phase Oxygen Atoms. *Surface Science* **2005,** *592* (1–3), 83-103.

54. Liang, Z.; Li, T.; Kim, M.; Asthagirl, A.; Weaver, J. F., Low-temperature activation of methane on the IrO2(110) surface. *Science* **2017,** *356* (6335), 298-301.

55. Farber, R. G.; Turano, M. E.; Oskorep, E. C. N.; Wands, N. T.; Juurlink, L. B. F.; Killelea, D. R., Exposure of Pt(553) and Rh(111) to atomic and molecular oxygen: do defects enhance subsurface oxygen formation? *J. Phys. Condens. Matter* **2017,** *29*, 164002.

56. Eren, B.; Liu, Z. Y.; Stacchiola, D.; Somorjai, G. A.; Salmeron, M., Structural Changes of Cu(110) and Cu(110)-(2 x 1)-O Surfaces under Carbon Monoxide in the Torr Pressure Range Studied with Scanning Tunneling Microscopy and Infrared Reflection Absorption Spectroscopy. *J. Phys. Chem. C* **2016,** *120* (15), 8227-8231.

57. Jones, T. E.; Rocha, T. C. R.; Knop-Gericke, A.; Stampfl, C.; Schlögl, R.; Piccinin, S., Insights into the Electronic Structure of the Oxygen Species Active in Alkene Epoxidation on Silver. *ACS Catalysis* **2015,** *5* (10), 5846-5850.

58. Altman, E. I.; Schwarz, U. D., Mechanisms, Kinetics, and Dynamics of Oxidation and Reactions on Oxide Surfaces Investigated by Scanning Probe Microscopy. *Adv. Mater.* **2010,** *22* (26-27), 2854-2869.

59. Badan, C.; Farber, R. G.; Heyrich, Y.; Koper, M. T. M.; Killelea, D. R.; Juurlink, L. B. F., Step-Type Selective Oxidation of Pt Surfaces. *The Journal of Physical Chemistry C* **2016,** *120* (40), 22927-22935.

60. Derouin, J.; Farber, R. G.; Killelea, D. R., Combined STM and TPD Study of Rh(111) Under Conditions of High Oxygen Coverage. *Journal of Physical Chemistry C* **2015,** *119*, 14748-14755.

61. Parker, D. H.; Bartram, M. E.; Koel, B. E., Study of High Coverages of Atomic Oxygen on the Pt(111) Surface. *Surface Science* **1989,** *217*, 489 - 510.

62. Bashlakov, D. L.; Juurlink, L. B. F.; Koper, M. T. M.; Yanson, A. I., Subsurface Oxygen on Pt(111) and Its Reactivity for CO Oxidation. *Catalysis Letters* **2012,** *142* (1), 1-6.

63. Lambert, R. M.; Williams, F. J.; Cropley, R. L.; Palermo, A., Heterogeneous alkene epoxidation: past, present and future. *Journal of Molecular Catalysis a-Chemical* **2005,** *228* (1-2), 27-33.

64. Grant, R. B.; Lambert, R. M., Mechanism of the Silver-Catalyzed Heterogeneous Epoxidation of Ethylene. *J. Chem. Soc., Chem. Commun.* **1983,** (12), 662-663.

65. Xu, Y.; Greeley, J.; Mavrikakis, M., Effect of subsurface oxygen on the reactivity of the Ag(111) surface. *J. Am. Chem. Soc.* **2005,** *127* (37), 12823-12827.

66. Gibson, K. D.; Viste, M.; Sanchez, E. C.; Sibener, S. J., High Density Adsorbed Oxygen on Rh(111) and Enhanced Routes to Metallic Oxidation Using Atomic Oxygen. *Journal of Chemical Physics* **1999,** *110* (6), 2757-2760.

67. Hinojosa, J. A., Jr.; Weaver, J. F., Surface structural evolution during the thermal decomposition of a PdO(101) thin film. *Surf. Sci.* **2011,** *605* (19-20), 1797-1806.

68. Derouin, J.; Farber, R. G.; Turano, M. E.; Iski, E. V.; Killelea, D. R., Thermally Selective Formation of Subsurface Oxygen in Ag(111) and Consequent Surface Structure. *ACS Catalysis* **2016**, 4640-4646.

69. Weaver, J. F.; Chen, J. J.; Gerrard, A. L., Oxidation of Pt(111) by gas-phase oxygen atoms. *Surf. Sci.* **2005,** *592* (1-3), 83-103.

70. Gibson, K. D.; Colonell, J. I.; Sibener, S. J., Velocity distributions of recombinatively desorbed O_2 originating from surface and subsurface oxygen/Rh(111). *Surf. Sci.* **1995,** *343* (1-2), L1151-L1155.

71. Kohler, L.; Kresse, G.; Schmid, M.; Lundgren, E.; Gustafson, J.; Mikkelsen, A.; Borg, M.; Yuhara, J.; Andersen, J. N.; Marsman, M.; Varga, P., High-coverage oxygen structures on Rh(111): Adsorbate repulsion and site preference is not enough. *Phys. Rev. Lett.* **2004,** *93* (26).

72. Huang, W. X.; Zhai, R. S.; Bao, X., Direct observation of subsurface oxygen on the defects of Pd(100). *Surf. Sci.* **1999,** *439*, L803 - L807.

73. van der Niet, M. J. T. C.; den Dunnen, A.; Juurlink, L. B. F.; Koper, M. T. M., A detailed TPD study of H2O and pre-adsorbed O on the stepped Pt(553) surface. *Phys. Chem. Chem. Phys.* **2011,** *13* (4), 1629-1638.

74. Umemoto, H.; Kusanagi, H.; Nishimura, K.; Ushijima, M., Detection of Radical Species Produced by Catalytic Decomposition of H_2, O_2 and Their Mixtures on Heated Ir Surfaces. *Thin Solid Films* **2009,** *517* (12), 3446-3448.

75. Umemoto, H.; Kusanagi, H., Catalytic decomposition of O_2, NO, N_2O and NO_2 on a heated Ir filament to produce atomic oxygen. *J. Phys. D: Appl. Phys.* **2008,** *41* (22), 225505.

76. van der Niet, M. J. T. C.; den Dunnen, A.; Juurlink, L. B. F.; Koper, M. T. M., The influence of step geometry on the desorption characteristics of O_2, D_2, and H_2O from stepped Pt surfaces. *J. Chem. Phys.* **2010,** *132* (17).

77. Jacobse, L.; den Dunnen, A.; Juurlink, L. B. F., The molecular dynamics of adsorption and dissociation of O_2 on Pt(553). *J. Chem. Phys.* **2015,** *143* (1), 014703.

78. Weaver, J. F.; Kan, H. H.; Shumbera, R. B., Growth and properties of high-concentration phases of atomic oxygen on platinum single-crystal surfaces. *J. Phys.-Condes. Matter* **2008,** *20* (18), 184015.

79. Devarajan, S. P.; Hinojosa, J. A., Jr.; Weaver, J. F., STM study of high-coverage structures of atomic oxygen on Pt(111): p(2 x 1) and Pt oxide chain structures. *Surf. Sci.* **2008,** *602* (19), 3116-3124.

80. McEwen, J. S.; Gaspard, P.; Mittendorfer, F.; de Bocarme, T. V.; Kruse, N., Field-assisted oxidation of rhodium. *Chem. Phys. Lett.* **2008,** *452* (1-3), 133-138.

81. Martin, N. M.; Klacar, S.; Gronbeck, H.; Knudsen, J.; Schnadt, J.; Blomberg, S.; Gustafson, J.; Lundgren, E., High-Coverage Oxygen-Induced Surface Structures on Ag(111). *Journal of Physical Chemistry C* **2014,** *118* (28), 15324-15331.

82. Gustafson, J.; Westerstrom, R.; Resta, A.; Mikkelsen, A.; Andersen, J. N.; Balmes, O.; Torrelles, X.; Schmid, M.; Varga, P.; Hammer, B.; Kresse, G.; Baddeley, C. J.; Lundgren, E., Structure and Catalytic Reactivity of Rh Oxides. *Catalysis Today* **2009,** *145* (3-4), 227-235.

83. Somorjai, G. A.; Park, J. Y., Molecular Surface Chemistry by Metal Single Crystals and Nanoparticles From Vacuum to High Pressure. *Chemical Society Reviews* **2008,** *37* (10), 2155-2162.

84. Fantauzzi, D.; Calderon, S. K.; Mueller, J. E.; Grabau, M.; Papp, C.; Steinruck, H. P.; Senftle, T. P.; van Duin, A. C. T.; Jacob, T., Growth of Stable Surface Oxides on Pt(111) at Near-Ambient Pressures. *Angewandte Chemie International Edition* **2017,** *56* (10), 2594-2598.

85. Devarajan, S. P.; Hinojosa Jr., J. A.; Weaver, J. F., STM Study of High-Coverage Structures of Atomic Oxygen on Pt(111): p(2 × 1) and Pt Oxide Chain Structures. *Surface Science* **2008,** *602* (19), 3116-3124.

86. Umemoto, H.; Kusanagi, H., Catalytic Decomposition of O_2, NO, N_2O, and NO_2 on a Heated Ir Filament to Produce Atomic Oxygen. *Journal of Physics D: Applied Physics* **2008,** *41* (22), 225505.

87. Kolb, M. J.; Farber, R. G.; Derouin, J.; Badan, C.; Calle-Vallejo, F.; Juurlink, L. B. F.; Killelea, D. R.; Koper, M. T. M., Double-Stranded Water on Stepped Platinum Surfaces. *Physical Review Letters* **2016,** *116* (13), 136101.

88. Kohler, L.; Kresse, G.; Schmid, M.; Lundgren, E.; Gustafson, J.; Mikkelsen, A.; Borg, M.; Yuhara, J.; Andersen, J. N.; Marsman, M.; Varga, P., High-Coverage Oxygen Structures on Rh(111): Adsorbate Repulsion and Site Preference is Not Enough. *Physical Review Letters* **2004,** *93* (26), 266103.

89. Klikovits, J.; Schmid, M.; Merte, L. R.; Varga, P.; Westerstrom, R.; Resta, A.; Andersen, J. N.; Gustafson, J.; Mikkelsen, A.; Lundgren, E.; Mittendorfer, F.; Kresse, G., Step-Orientation-Dependent Oxidation: From 1D to 2D Oxides. *Physical Review Letters* **2008,** *101*, 266104.

90. Dudin, P.; Barinov, A.; Gregoratti, L.; Kiskinova, M.; Esch, F.; Dri, C.; Africh, C.; Comelli, G., Initial Oxidation of a Rh(110) Surface Using Atomic or Molecular Oxygen and Reduction of the Surface Oxide by Hydrogen. *Journal of Physical Chemistry B* **2005,** *109* (28), 13649-13655.

91. Mittendorfer, F., Low-Dimensional Surface Oxides in the Oxidation of Rh Particles. *Journal of Physics: Condensed Matter* **2010,** *22*, 393001.
92. Ganduglia-Pirovano, M. V.; Scheffler, M.; Baraldi, A.; Lizzit, S.; Comelli, G.; Paolucci, G.; Rosei, R., Oxygen-Induced Rh 3d5/2 Surface Core-Level Shifts on Rh(111). *Physical Review B* **2001,** *63* (20), 205415.

93. Goodman, D. W., Correlations between surface science models and "real-world" catalysts. *Journal of Physical Chemistry* **1996,** *100* (31), 13090-13102.

94. Gao, F.; McClure, S.; Chen, M.; Goodman, D. W., Comment on "Catalytic Acitivty of the Rh Surface Oxide: CO Oxidation over Rh(111) under Realistic Conditions". *The Journal of Physcial Chemistry C* **2010,** *114* (50), 22369-22371.

95. Gustafson, J.; Westerstrom, R.; Balmes, O.; Resta, A.; van Rijn, R.; Torrelles, X.; Herbschleb, C. T.; Frenken, W. M.; Lundgren, E., Reply to "Comment on 'Catalytic Activity of the Rh Surface Oxide: CO Oxidation over Rh(111) under Realistic Conditions'". *The Journal of Physcial Chemistry C* **2010,** *114* (50), 22372-22373.

96. Jaworowski, A. J.; Beutler, A.; Strisland, F.; Nyholm, R.; Setlik, B.; Heskett, D.; Andersen, J. N., Adsorption sites in O and CO coadsorption phases on Rh(111) investigated by high-resolution core-level photoemission. *Surface Science* **1999,** *431* (1-3), 33-41.

97. Hopstaken, M. J. P.; Niemantsverdriet, J. W., Structure sensitivity in the CO oxidation on rhdoium: Effect of adsorbate coverages on oxidation kinetics on Rh(100) and Rh(111). *Journal of Chemical Physics* **2000,** *113* (13), 5457-5465.

98. Krenn, G.; Bako, I.; Schennach, R., CO adsorption and CO and O coadsorption on Rh(111) studied by reflection absorption infrared spectroscopy and density functional theory. *Journal of chemical physics.* **2006,** *124* (14), 144703.

99. Kizilkaya, A. C.; Gracia, J. M.; Niemantsverdriet, J. W., A Direct Relation between Adsorbate Interactions, Configurations, and Reactivity: CO Oxidation on Rh(100) and Rh(111). *The Journal of Physcial Chemistry C* **2010,** *114* (49), 21672-21680.

100. McClure, S.; Lundwall, M.; Yang, F.; Zhou, Z.; Goodman, D. W., CO Oxidation on Rh/SiO2/Mo(112) Model Catalysts at Elevated Pressures. *The Journal of Physcial Chemistry C* **2009,** *113* (22), 9688-9697.

101. Lambeets, S. V.; Barroo, C.; Owczarek, S.; Jacobs, L.; Genty, E.; Gilis, N.; Kruse, N.; de Bocarme, T. V., Adsorption and Hydrogenation of CO2 on Rh Nanosized Crystals: Demonstration of the Role of Interfacet Oxygen Spillover and Comparative Studies with O2, N2O, and CO. *The Journal of Physcial Chemistry C* **2017,** *121*, 16238-16249.

102. Cernota, P.; Rider, K.; Yoon, H. A.; Salmeron, M.; Somorjai, G., Dense structures formed by CO on Rh(111) studied by scanning tunneling microscopy. *Surface Science* **2000,** *445*, 249-255.
103. Derouin, J.; Farber, R. G.; Turano, M. E.; Iski, E. V.; Killelea, D. R., Thermally Selective Formation of Subsurface Oxygen in Ag(111) and Consequent Surface Structure. *ACS Catalysis* **2016,** *6* (7), 4640-4646.

VITA

Rachael G. Farber was born in Hartford, Connecticut, and raised in Grosse Pointe, Michigan. Before attending Loyola University Chicago, she attended Case Western Reserve University, where she earned a Bachelor of Science in Chemistry, in 2013.

While at Loyola, Rachael was awarded the 2016 Denkewalter Poster Prize, the Arthur J. Schmitt Dissertation Fellowship for the 2017-2018 academic year, the Nellie Yeoh Whetten Award and the Morton M. Traum Surface Science Student Award at the AVS 64th International Symposium and Exhibition in November 2017, and was elected chair of the 2017 Gordon Research Seminar-Dynamics at Surfaces. Rachael was also invited to present her research during a Loyola University Chicago Department Seminar as well as at Leiden Institute of Chemistry, Catalysis and Surface Chemistry, in the Netherlands.

Currently, Rachael is preparing for a postdoctoral position under Prof. Steven J. Sibener at The University of Chicago, beginning on May 14th, 2018.